

**1 Delayed Freshwater Export from a ~~Greenlandic~~ Greenland tidewater glacial**  
**2 fjord**

**3** Robert Sanchez,<sup>a</sup> Donald Slater,<sup>b</sup> and Fiammetta Straneo,<sup>a</sup>

**4** <sup>a</sup> *Scripps Institution of Oceanography, UC San Diego, San Diego, California*

**5** <sup>b</sup> *School of Geosciences, University of Edinburgh, Edinburgh, United Kingdom*

**6** *Corresponding author:* Robert Sanchez, rmsanche@ucsd.edu

7 ABSTRACT: Freshwater from the Greenland Ice Sheet is routed to the ocean through narrow  
8 fjords along the coastline where it impacts ecosystems both within the fjord and on the continental  
9 shelf, regional circulation, and potentially the global overturning circulation. However, the timing  
10 of freshwater export is sensitive to the residence time of waters within glacial fjords. Here, we  
11 present evidence of seasonal freshwater storage in a tidewater glacial fjord using hydrographic and  
12 velocity data collected over 10 days during the summers of 2012 and 2013 in Saqqaq (SQ),  
13 a mid-size fjord in West Greenland. The data revealed a rapid freshening trend of  $-0.05 \pm 0.01$   
14 g/kg/day and  $-0.04 \pm 0.01$  g/kg/day, in 2012 and 2013, respectively, within the intermediate layer  
15 of the fjord (15- 100 m) less than 2.5 km from the glacier terminus. The freshening trend is  
16 driven, in part, by the downward mixing of outflowing glacially-modified water near the surface  
17 and increasingly stratifies the fjord from the surface downwards over the summer melt season. We  
18 construct a box model which recreates the first-order dynamics of the fjord and describes freshwater  
19 storage as a balance between friction and density-driven exchange outside the fjord. The model  
20 can be used to diagnose the timescale for this balance to be reached, and for SQ we find a month  
21 lag between subglacial meltwater discharge and net freshwater export. These results indicate a  
22 fjord-induced delay in freshwater export to the ocean that should be represented in large-scale  
23 models seeking to understand the impact of Greenland freshwater on the regional climate system.

24 **1. Introduction**

25 Mass loss from the Greenland Ice Sheet is predicted to accelerate during the 21st century,  
26 further contributing to sea level rise and with downstream consequences on ocean circulation  
27 and ecosystems (Bamber et al. 2019; Goelzer et al. 2020; Böning et al. 2016; Frajka-Williams  
28 et al. 2016; Arrigo et al. 2017; Oksman et al. 2022). Freshwater fluxes from the ice sheet are  
29 discharged in the form of both solid and liquid forms contributing cumulatively  $7700 \pm 460 \text{ km}^3$   
30 and  $8400 \pm 1680 \text{ km}^3$  of freshwater respectively, from 2000-2016 (Bamber et al. 2018). The  
31 freshwater and its dissolved and particulate chemical content are released into long and narrow  
32 fjords before being routed onto the continental shelves where they can affect regional circulation,  
33 salinity, biogeochemistry and potentially large-scale deep convection, although recent evidence  
34 suggests Greenland's freshwater might remain close to the coast (Straneo and Cenedese 2015;  
35 Böning et al. 2016; Frajka-Williams et al. 2016; Thornalley et al. 2018; Hendry et al. 2021; Le Bras  
36 et al. 2021). The freshwater from glaciers also impacts regional ecosystems through both the direct  
37 injection of nutrients and the upwelling of ambient deep nutrients leading to highly productive  
38 fjords and fisheries (Cape et al. 2019; Meire et al. 2016a,b, 2017; Hopwood et al. 2020) that are,  
39 therefore, sensitive to future changes in freshwater fluxes (Hopwood et al. 2018; Oliver et al. 2020).  
40 The impact of freshwater will vary depending on how, when and where it mixes with seawater.  
41 This mixing is in turn affected by fjord circulation and stratification (Mortensen et al. 2011, 2020).  
42 Therefore, determining how fjord dynamics alter the distribution and export of freshwater is crucial  
43 to understanding the impact of the Greenland Ice Sheet on the ocean and ecosystems.

44 The liquid component of freshwater enters fjords in three forms: (i) through direct melting of  
45 ice by the ocean (submarine meltwater; SMW), (ii) meltwater from the ice sheet surface that has  
46 drained to the ice sheet base and enters the fjord from beneath a glacier (subglacial meltwater  
47 discharge; SGD), and (iii) meltwater from the ice sheet surface that has not drained to the base  
48 and enters the fjord at the surface (meltwater runoff). Since it is expected that the ~~vast~~ majority of  
49 surface meltwater does drain to the ice sheet base in this system, and since this study excludes the  
50 surface layers of the fjord, we here make no further mention of meltwater runoff. SMW fluxes are  
51 sensitive to ocean heat and released at various depths along the face of the terminus. Additionally,  
52 SMW is produced by melting icebergs as they transit through the fjord. Meltwater drained as  
53 SGD is buoyant ~~–~~ and produces turbulent plumes which entrain ambient water and drive a strong

54 overturning circulation within the fjord (Straneo and Cenedese 2015; Carroll et al. 2017). This  
55 overturning circulation, along with tidal flows and shelf-forced fluctuations, drives horizontal and  
56 vertical mixing within the fjord and determines the exchange of freshwater with the shelf (Zhao  
57 et al. 2021). However, the transport and outflow depth of the SGD plume is sensitive to fjord  
58 stratification, resulting in a complex feedback between fjord circulation and freshwater content  
59 (De Andrés et al. 2020).

60 Glacial fjords are often described as being in one of two states, a winter state with decreased  
61 stratification and a shelf-influenced circulation, and a summer state with increased stratification and  
62 a strong plume-driven circulation (Jackson and Straneo 2016; Gladish et al. 2014; Mortensen et al.  
63 2014). These dramatic differences in circulation and stratification can lead to a seasonal description  
64 of glacial fjords that overlooks the dynamic evolution of fjords within a season. Additionally, the  
65 challenges of obtaining measurements in ice-congested fjords often limit field campaigns to short-  
66 duration summer surveys (Stevens et al. 2016; Beard et al. 2015, 2017; Cape et al. 2019; Motyka  
67 et al. 2011; Wood et al. 2018; Moon et al. 2018; Inall et al. 2014; Bendtsen et al. 2015, 2021;  
68 Muilwijk et al. 2022). While these surveys provide invaluable snapshots of heat, nutrient, and  
69 meltwater fluxes, it is often assumed that the data are representative of the whole summer and some  
70 heat budgets explicitly assume the fjord is in a “steady state” or use a single summer average (Inall  
71 et al. 2014; Jackson and Straneo 2016).

72 However, a limited number of observations have shown significant subseasonal variability of  
73 hydrographic properties in fjords (Stuart-Lee et al. 2021; Carroll et al. 2018; Mortensen et al.  
74 2014, 2013, 2018; Meire et al. 2016b; Mernild et al. 2015). For example, Mortensen et al. (2011,  
75 2014, 2018) show that Godthåbsfjord freshens and the isopycnals deepen throughout the summer,  
76 suggesting that fjord processes modulate the timing and vertical distribution of freshwater export.  
77 This is in contrast to the approach of large-scale ocean models, which often input freshwater  
78 from glacial freshwater at the surface and assume the transit time of meltwater through fjords is  
79 negligible (Arrigo et al. 2017; Dukhovskoy et al. 2019). To further understand the subseasonal  
80 evolution of glacial fjords and their impact on freshwater export, we use a dataset of high-frequency  
81 hydrographic and velocity observations collected over 10 days during each of the summers of  
82 2012 and 2013 in [Sarqardleq Fjord](#)[Saqqarleq](#), a mid-size fjord in west Greenland associated with  
83 [Sarqarliup Saqqarliup Sermia](#) glacier. The data revealed a rapid freshening trend of 0.05 g/kg/day

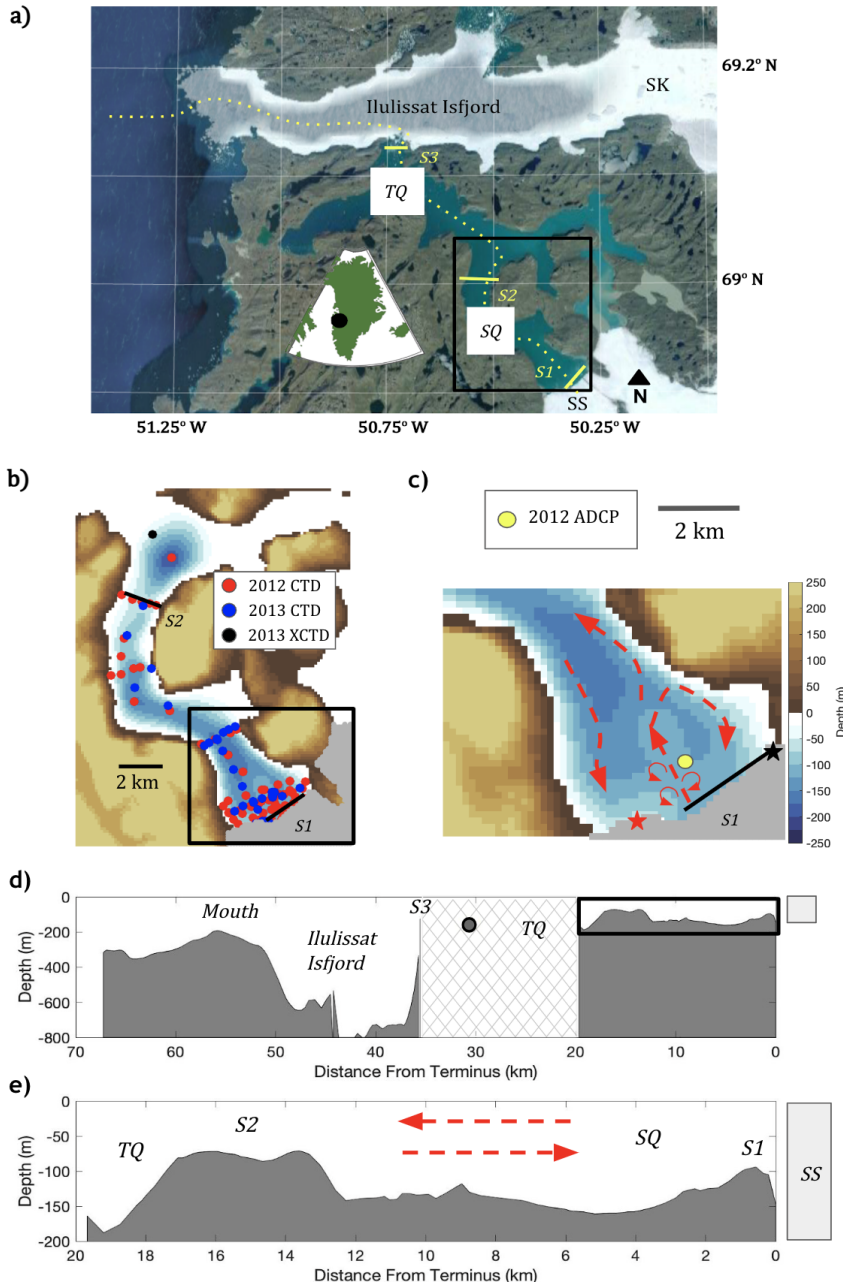
and 0.04 g/kg/day, in 2012 and 2013 respectively, within the intermediate layer of the fjord less than 2.5 km from the glacier. These freshening trends were of similar magnitude despite the fact that 2012 was a year of record surface melt and 2013 was an average melt year. The freshening indicates that SMW and SGD from the glacier is stored within the fjord leading to a transformation of fjord waters and a delay in the net export of freshwater. A box model is developed to elucidate the storage and release dynamics of the glacial fjord. The box model is formulated for ~~Sarqardleq~~Saqqarleq, but is generic and can be applied to other systems. Our results suggest that Greenland's glacial fjords are nonsteady and respond rapidly to the input of ice sheet meltwater. The freshwater storage results in a lag of peak freshwater export from the glacier to the ocean that needs to be accounted for in any regional or global ocean model that does not resolve fjords and fjord processes.

## 2. Setting, Data and Methods

### a. Setting and Background

We investigate changes within ~~Sarqardleq Fjord~~(SF)~~Saqqarleq~~(SQ), a mid-sized glacial fjord in west Greenland associated with the glacier ~~Sarqarliup~~Saqqarliup Sermia, during a period of sustained SGD. ~~SF~~SQ is the southern arm of the Ilulissat ~~Ieefjord~~Isfjord system which connects Sermeq Kujalleq (commonly referred to as Jakobshavn Isbrae) with Disko Bay (Fig. 1a). ~~SF~~SQ has a broad sill (S1) about 500 m from the grounding line isolating the glacier from the deepest ~~SF~~SQ waters. This sill varies in depth from 50 m at its southwest end to 100 m at its deepest point. The fjord varies in width from about 6 km at the head of the fjord, to 2.2 km in the main channel of the fjord before it connects to Tasiussaq ~~Fjord~~(TF)~~(TQ)~~ and then Ilulissat ~~Ieefjord~~Isfjord. ~~SF and TF~~SQ and TQ are separated by an 80 m deep sill (S2) that is 16 km downfjord of ~~Sarqarliup Glacier, and TF~~Saqqarliup Sermia, and TQ is separated from Ilulissat ~~Ieefjord~~Isfjord by a 125 m deep sill (S3). The sill between ~~TF~~TQ and Ilulissat prevents the deeper relatively warm basin waters of Ilulissat from reaching ~~SFSQ~~.

~~SF~~SQ lacks a thick ice ~~melange~~mélange, unlike major glacial fjords such as Ilulissat ~~Ieefjord and Sermilik~~FjordIsfjord and Sermilik, which enables measurements to be made within 200 m of the terminus and makes ~~SF~~SQ ideal for field studies of ice-ocean interactions (Stevens et al. 2016; Mankoff et al. 2016; Slater et al. 2018; Wagner et al. 2019; De Andrés et al. 2020). SGD enters the fjord from below the glacier at two locations, a primary plume located 2.3 km along the



108 FIG. 1. a) A regional map of Saqqarleq Fjord Saqqarleq (SFSQ) and Tasiussaq Fjord (TFTQ) and Ilulissat  
 109 Isfjord showing sill locations and nearby glaciers Saqqarliup Saqqarliup Sermia (SS) and Sermeq Kujalleq (SK).  
 110 The inset map shows the location of SF-SQ within the Greenland continent. The yellow dashed line is the  
 111 bathymetry slice shown in (d) and (e). b) Map of SF-SQ with the locations of CTDs collected in 2012 (red),  
 112 2013 (blue) and a 2013 XCTD (black). c) Close-up of the area near the terminus of SS with bathymetry and  
 113 a schematic of the circulation. The locations of the primary plume (red star) and secondary plume (black star)  
 114 based on Stevens et al. (2016) are shown along with the location of a moored ADCP (Fig. 7). d) An along-track  
 115 bathymetry profile created using BedMachine4 (Morlighem et al. 2017). Cross hatching fills the region where  
 116 data is unreliable. A circle marks the single depth point available, taken from a 2013 XCTD profile. e) A close-up  
 117 of the bathymetry of SF-SQ noting the major sills, glacier, and a schematic of the overturning circulation.

terminus from the southwest corner and a secondary plume 4.5 km along the terminus [Fig. 1c, (Stevens et al. 2016)]. The secondary plume is associated with substantially weaker SGD resulting in a deeper neutral buoyancy depth (Stevens et al. 2016; De Andrés et al. 2020). A remote-control kayak equipped with a depth-varying CTD sampled within the surface expression of the primary plume in 2013, finding that the plume was composed of 90% entrained ambient water, 10% SGD and less than 0.1% SMW (Mankoff et al. 2016). Along-fjord transects of temperature and velocity revealed that after surfacing, the plume submerged and flowed out as a subsurface jet (Mankoff et al. 2016). A high-resolution simulation of [SFSQ](#), constrained with observations from 2013, found that the plume-turned-jet impinged on the fjord wall and generated a vigorous terminus-scale wide recirculation generating widespread melting of the glacier terminus [Fig. 1c, (Slater et al. 2018)].

Previously, De Andrés et al. (2020) used parts of this dataset to explore differences in the surface emergence of a subglacial plume across two consecutive years, including one in a year with record SGD (2012). They found that greater cumulative SGD was associated with increased fjord stratification which, in turn, exerted a dominant influence on plume height. They did not investigate, however, the physical mechanisms controlling the stratification and the potential impacts this stratification has on the export of freshwater.

### *b. Data*

Conductivity, Temperature and Depth (CTD) profiles were collected from a small boat in the fjord from 17-27 July in 2012 and 23 July - 1 August 2013 (Fig. 1b). The profiles were collected using an RBR XR 620 CTD and averaged into 1 dbar bins. 90 casts were collected in 2012 and 96 casts were collected in 2013. In 2012 (2013), 51 (59) of the casts extended to at least 100 m and only these deeper casts were used in our hydrographic analysis. Additionally in 2013, a Sippican eXpendable CTD (XCTD) was collected just outside the 80 m deep S2 in [TFTQ](#). The data are presented in Conservative Temperature ( $\Theta$  or temperature), Absolute Salinity ( $S$  or salinity) and Potential Density [ $\rho$  or density; (McDougall and Barker 2011)] with stratification defined using the Brunt-Väisälä frequency

$$N^2 = -\frac{g}{\rho_{ref}} \frac{d\rho}{dz}, \quad (1)$$

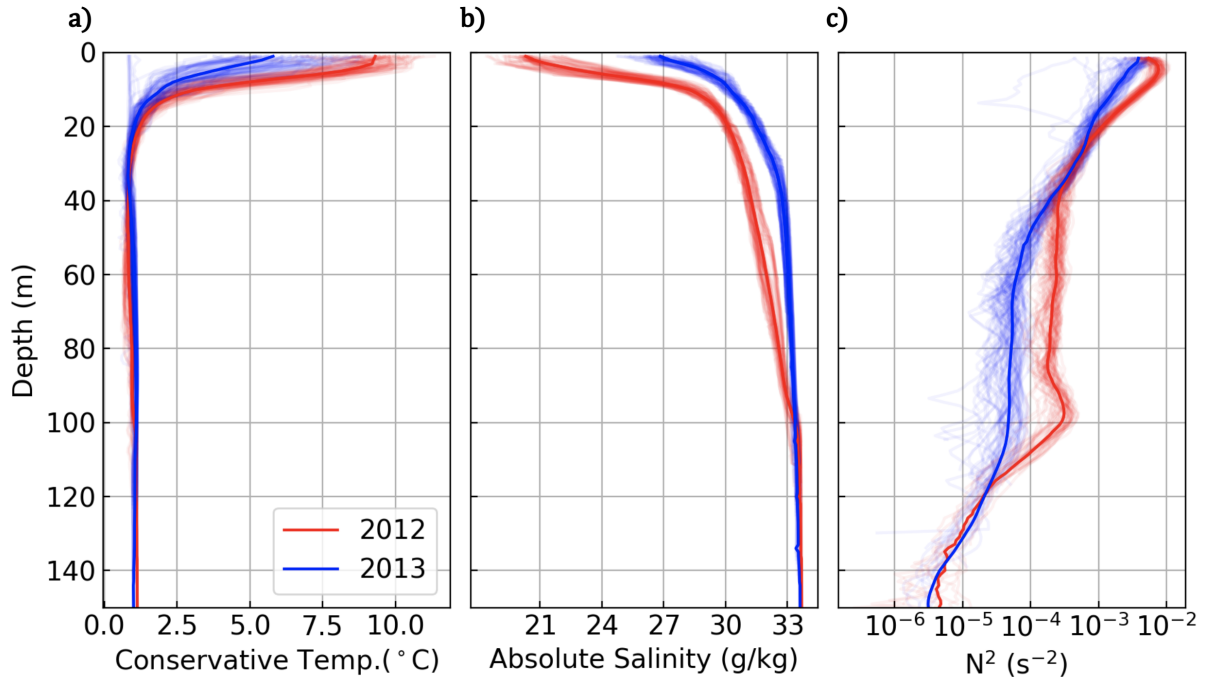
where  $g$  is gravitational acceleration and  $\rho_{ref} = 1026 \text{ kg/m}^3$  is a reference density.

150 An upward-looking moored Teledyne RDI 300 kHz Acoustic Doppler Current Profiler (ADCP)  
151 was deployed 1.6 km from the terminus (Fig. 1c) and collected velocity data from July 2012 - April  
152 2013. The ADCP was deployed on the seafloor at ~~125~~114 m and recorded velocity in 4 m bins  
153 from 6 m to ~~144~~102 m, after removing the top two 6 m for side-lobe effects. The barotropic tide  
154 was estimated from a pressure sensor, the Arctic Ocean Inverse Tide Model (Padman and Erofeeva  
155 2004; Erofeeva and Egbert 2020) when data was unavailable, and subtracted from the ADCP data  
156 (Sup. Fig. 1). The estimates of SGD entering the fjord are taken from the Modele Atmospherique  
157 Regional [MAR;(Fettweis et al. 2017; Delhasse et al. 2020)] with the dataset provided by Mankoff  
158 et al. (2020). We also use salinity values collected from seals as reported in Mernild et al. (2015)  
159 and calibrate them against our CTD data (Sup. Fig. 2).

### 160 3. Analysis of Observational Data

#### 161 a. Background Hydrography

162 The hydrography of ~~SF SQ~~ has been investigated by De Andrés et al. (2020) and Stevens et al.  
163 (2016), but a brief description is necessary here to provide context for our analysis. ~~The During~~  
164 summer, the fjord can be approximated as a three-layer system with a surface layer approximately  
165 10-15 m deep, an intermediate layer between 15 - 100 m deep and a homogeneous layer deeper than  
166 100 m (~~DWBW~~, Fig. 2). Temperature profiles (Fig. 2a), reveal a warm surface layer, presumably  
167 from solar heating, and a colder layer extending from 15 m to the bottom. There is little difference  
168 in temperature between the second and third layer. Interannual differences between 2012 and 2013  
169 are small with mean temperatures below the surface layer of 0.9 °C and 1 °C respectively. Salinity  
170 profiles (Fig. 2b), show that the intermediate layer of the fjord is substantially fresher in 2012  
171 (mean salinity 31.9 g/kg) than in 2013 (32.9 g/kg). The interannual differences in salinity are  
172 consistent with 2012 being a year of record ice sheet surface melt (Nghiem et al. 2012; Tedesco  
173 et al. 2013). Below 100 m in the ~~deep basin~~ layer, the salinity between the two years are similar.  
174 This evidence suggests that S1 blocks the majority of glacial water from reaching the ~~deep basin~~  
175 layer and that ~~DW BW is~~ primarily composed of waters unmodified by SS and imported from  
176 outside of the fjord, similar to the deep basin waters of some shallow-silled glacial fjords (Hager  
177 et al. 2022). This basin water has characteristics of diluted Baffin Bay Polar Water, one of the two



180 Fig. 2. a) Conservative Temperature versus depth (red 2012, blue 2013). b) Absolute Salinity. c) Stratification  
 181 ( $N^2$ ) over the top 150 m. In all profiles the mean profile is given in bold. The stratification profiles are low-pass  
 182 filtered over a window of 10 m to remove noise. The x-axis in panel c is logarithmic.

178 water masses found in Greenland north of Davis Strait (Gladish et al. 2014; Stevens et al. 2016;  
 179 Rysgaard et al. 2020; Mortensen et al. 2022).

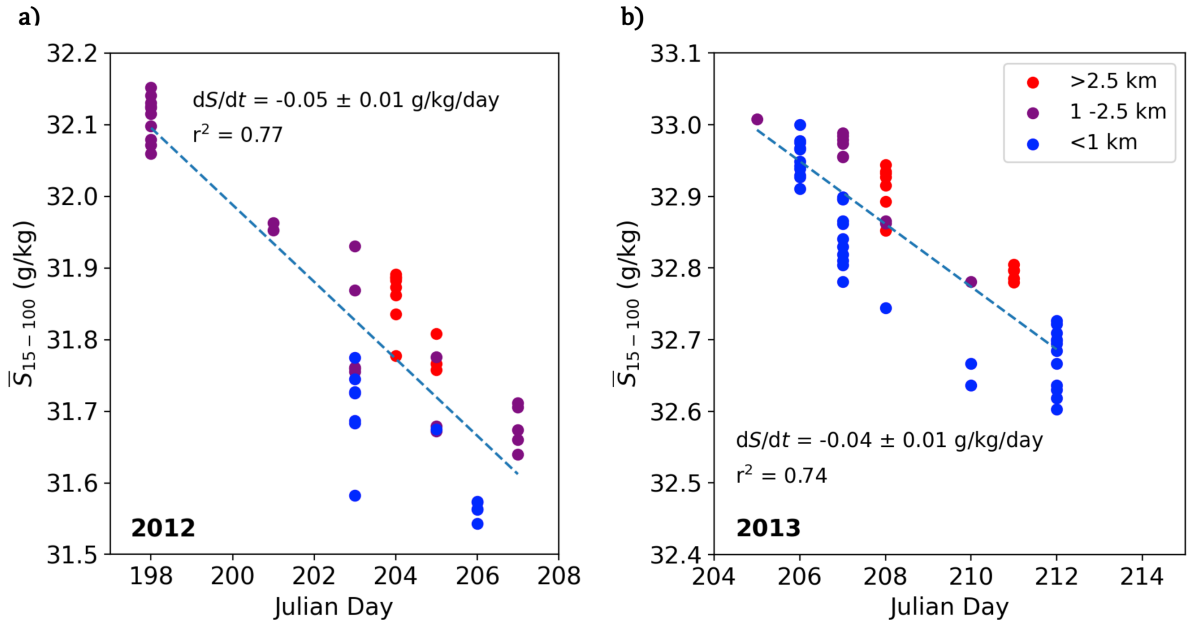
183 The density in SFSQ is dominated by salinity, and the stratification profiles reveal that decreased  
 184 salinity above 100 m is associated with increased vertical density gradients (Fig. 2). In both years,  
 185 the stratification exhibits peaks around the surface layer but decreases with depth. Above 40 m,  
 186 the mean stratification was approximately double in 2012 ( $2 \times 10^{-3} s^{-2}$ ) compared to 2013 ( $1 \times$   
 187  $10^{-3} s^{-2}$ ). The mean stratification between 40 to 100 m is about 4 times higher in 2012 ( $2.7 \times 10^{-4}$   
 188  $s^{-2}$ ) compared to 2013 ( $0.07 \times 10^{-4} s^{-2}$ ). The profiles in 2012 also exhibit a peak in stratification  
 189 just above the homogeneous layer (100 m) before converging to the 2013 properties reflecting the  
 190 presence of sill S2.

191 *b. Continuous Fjord Freshening*

192 We find that ~~SF-SQ~~ gets fresher during the summer field campaign in both years indicating it is  
193 not in steady state. We analyze freshwater storage by examining temporal trends in salinity within  
194 layers of the fjord. We focus on the intermediate layer (15-100 m depth) because the surface layer  
195 shows a high degree of variability, presumably, imparted by processes that are not the focus of this  
196 study, such as ~~land runoff and solar insolation~~. runoff (meltwater, land and precipitation) and solar  
197 insolation (Sup Fig. 4). While these surface processes are important, strong stratification ( $N^2 \approx$   
198  $10^{-2} \text{ s}^{-2}$ ) likely limits their impact at depth in this system. In both 2012 and 2013, the mean salinity  
199 over the intermediate layer continuously decreased over the course of each field campaign (Fig. 3).  
200 The mean salinity also exhibited an along-fjord trend with fresher waters closer to the glacier, but  
201 the temporal trend is greater than the longitudinal trend. We can thus rule out that the freshening is  
202 due to the advection of freshwater from Ilulissat ~~Ieefjord~~ Isfjord as otherwise the salinity gradient  
203 would be reversed. The freshening trend in 2012 is  $-0.05 \pm 0.01 \text{ g/kg/day}$  ( $r^2 = 0.77$ ) and in 2013  
204 is  $-0.04 \pm 0.01 \text{ g/kg/day}$  ( $r^2 = 0.74$ ), with uncertainty defined using a bootstrapping method. This  
205 trend is consistent with a moored CTD at 70 m that recorded salinity continuously over this time  
206 period (Sup. Fig 3). The CTD data is concentrated near the head of ~~Sarqardleq Fjord~~ SQ where  
207 mixing is likely to be most intense (Bendtsen et al. 2021) and therefore it is unclear how close to  
208 the shelf the freshening trend persists. The jet from the glacier outflows at around 20 m depth, but  
209 the freshening occurs at all depths (Sup. Fig. 4) suggesting that either the outflowing freshwater is  
210 being vertically mixed downwards or strong submarine melting is freshening waters at all depths.

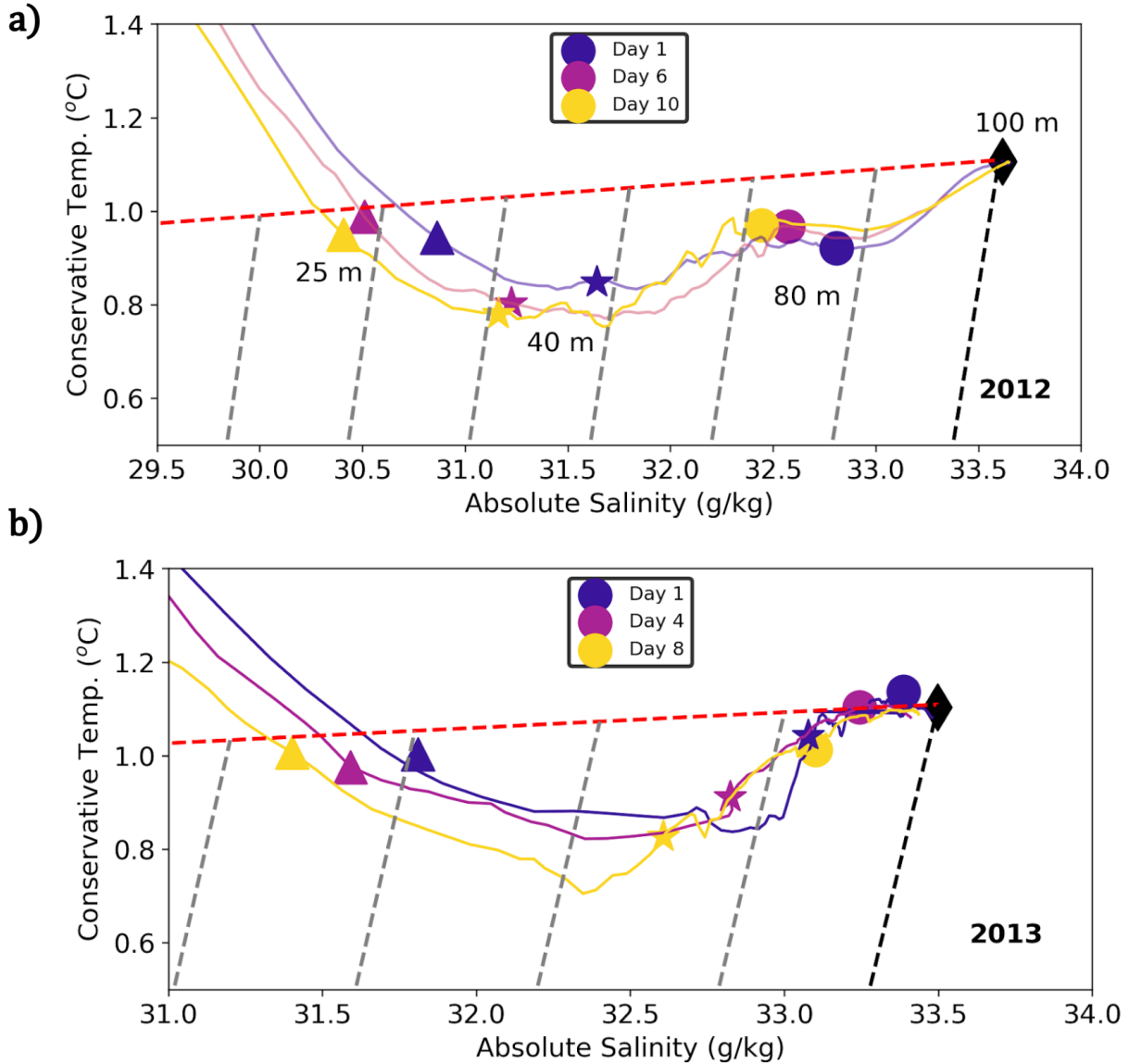
214 *c. Subglacial Meltwater Discharge is the Dominant Freshwater Source*

215 Next, we show that the freshening trend is due to an increase in SGD content in the water column.  
216 We can visually identify which freshwater source is responsible using a temperature and salinity  
217 (TS) diagram with the depths 25 m, 40 m, 80 m and 100 m highlighted in Figure 4. The profiles  
218 shown are representative of the start, middle and end of the field campaign and were all collected  
219 from approximately the same distance from the glacier. By looking at the change in temperature  
220 associated with freshening we can determine the source of freshwater. For example, we expect  
221 freshening driven by SMW to be associated with a substantial cooling of water while freshening due  
222 to SGD is associated with a much smaller change in temperature. In 2012, the change in properties



211 Fig. 3. a) Mean Absolute Salinity of 2012 CTD profiles from 15 m - 100 m (surface layer to S2 depth) with a  
 212 best fit trend. Colors indicate distance from terminus. X-axis is the day of the field campaign. b) same but for  
 213 2013.

223 at each depth are roughly parallel to the subglacial meltwater discharge-mixing line indicating that  
 224 the freshening is due to an increase in SGD at depth rather than SMW. However in 2013, only the  
 225 properties at 25 m appear parallel to the subglacial meltwater discharge-mixing lines while deeper  
 226 water appears to be on a slope between the subglacial meltwater discharge-mixing line and the  
 227 submarine melt-mixing-melt line. Following the procedure of Mankoff et al. (2016) and Mortensen  
 228 et al. (2020) (see Supplemental) we use a water-mass analysis to quantify changes in the relative  
 229 concentration of SGD and SMW (Table 1). The fraction of SGD significantly increased by around  
 230 1% in both years ( $p < 10^{-4}$  for all cases). Changes in the fraction of SMW were mostly significant  
 231 ( $p < 10^{-4}$  for all cases except 2013 at 25 m), but varied with decreases (2012) or increases (2013)  
 232 around 0.1 %. In both years the increase in SGD is an order of magnitude higher than changes in  
 233 SMW. Thus while SMW is present, we conclude that the freshening trend is being driven primarily  
 234 by the accumulation of SGD. This process must occur from the top down as SGD is exported in  
 235 the jet which outflows around 20 m depth (Mankoff et al. 2016; Slater et al. 2018).



236 FIG. 4. a) TS diagram of days 1, 4, and 10 in 2012 with the depths 25 (triangles), 40 (stars), 80 (circles) and  
 237 100 m (diamond) highlighted with symbols. b) Same as a but for 2013, the final point is from day 8 rather than  
 238 day 10. On top of the TS diagram, we plot a subglacial meltwater discharge-mixing line (red) which represents  
 239 the mixing between SGD ( $S = 0 \text{ g/kg}$ ,  $\Theta = 0 \text{ }^{\circ}\text{C}$ ) and water at 100 m. There are also submarine melt-mixing-melt  
 240 lines (gray lines), or Gade slopes, which represent a hypothetical mixture of DW-BW and SMW ( $S = 0$ ,  $\Theta = -87$   
 241  $^{\circ}\text{C}$ )

242 *d. Interannual Subglacial Meltwater Discharge Differences*

243 Comparison of SGD timeseries from MAR highlights that SGD flux into the fjord was substan-  
 244 tially higher in 2012 than in 2013 (Fig. 5). In 2012, the SGD flux into the fjord started about

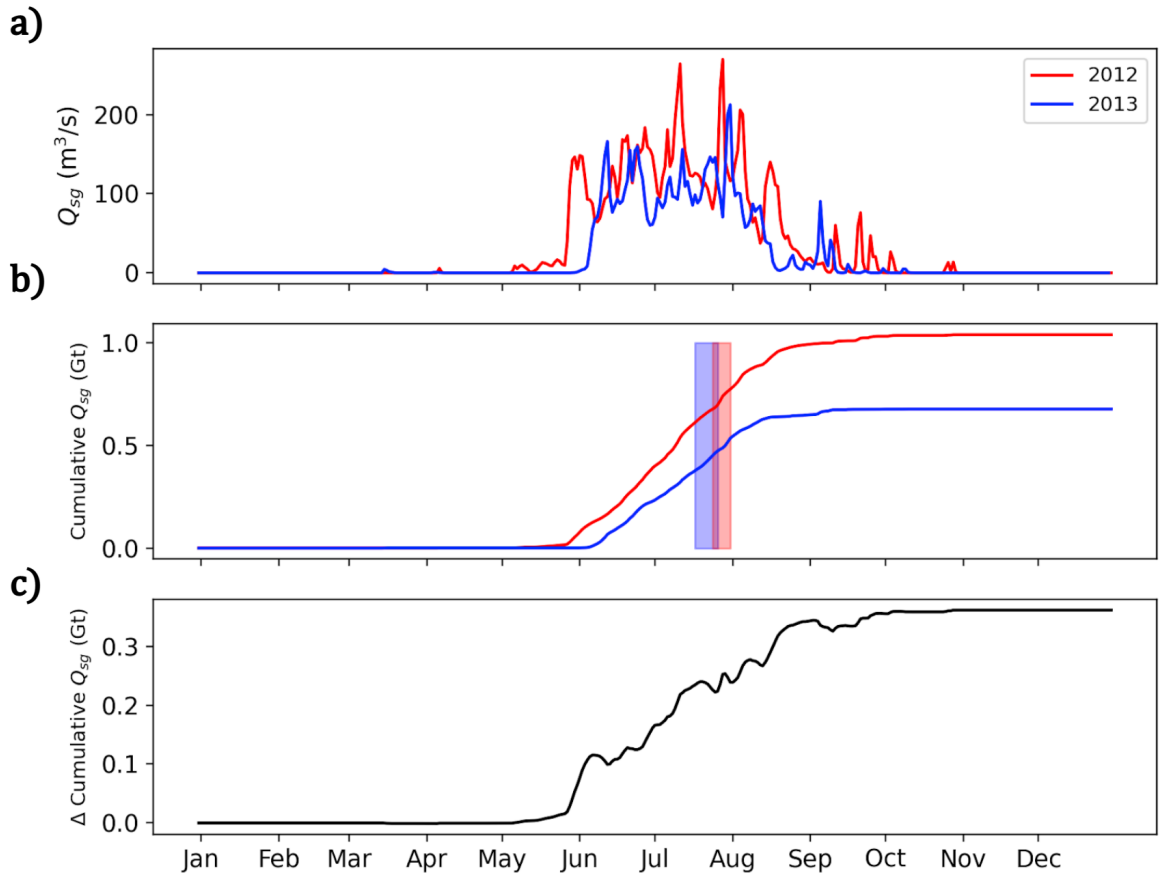
TABLE 1. Change in freshwater concentration of SGD and SMW from day 1-10 in 2012 and day 1-8 in 2013.

Depth	2012 ΔSMW	2012 ΔSGD	2013 ΔSMW	2013 ΔSGD
25 m	-0.06 ± 0.03 %	1.5 ± 0.2 %	0.02 ± 0.03 %	1.4 ± 0.3 %
40 m	0.08 ± 0.02 %	1.3 ± 0.1 %	0.11 ± 0.05 %	1.0 ± 0.1 %
80 m	-0.08 ± 0.01 %	1.1 ± 0.1 %	0.06 ± 0.03 %	0.4 ± 0.1 %

245 10 days earlier and the mean flux during the period of sustained SGD (DOY 160 - 215) was 138  
 246  $\text{m}^3/\text{s}$  compared to  $111 \text{ m}^3/\text{s}$  in 2013 (Fig. 5a). This increased SGD flux resulted in cumulative  
 247 freshwater input that was 40% higher in 2012 by the end of summer (Fig. 5b). The difference in  
 248 cumulative SGD grew throughout the summer, such that by the end of the respective field seasons,  
 249 0.3 Gt more freshwater had entered in the fjord in 2012 than 2013 (Fig. 5c)

253 *e. Density differences across the outer sill (S2)*

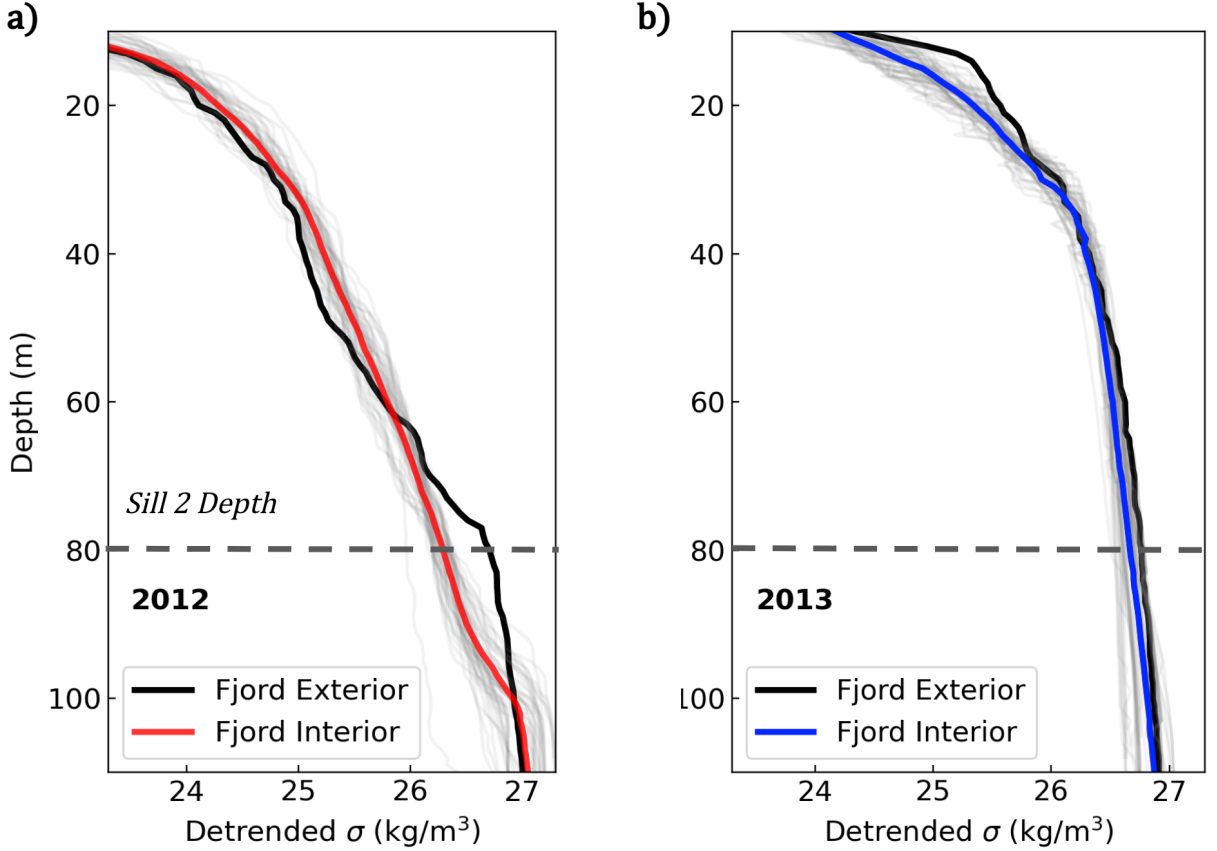
254 Comparison of CTD profiles from inside and outside of ~~SF-SQ~~ shows how the increase in  
 255 stratification in the inner fjord driven by SGD leads to greater interaction with topography (Fig.  
 256 6). In 2012, a density difference arose between the fjord interior and exterior near the depth of S2  
 257 (80 m), which separates ~~SF from TFSQ from TQ~~. Below this sill depth, the outside profile was less  
 258 stratified and more dense than profiles within the fjord (Fig. 6a). This feature is not evident in 2013  
 259 (Fig. 6b). Note that all profiles have had the linear temporal trend in salinity (Fig. 3) removed  
 260 so that we can compare profiles taken on different days. Only a single cast was available from  
 261 outside of the fjord in 2012, and only 2 profiles in 2013, however the density is outside the range  
 262 of variability observed within the fjord, so the feature is less likely to be transient. The density  
 263 difference which is centered at the sill depth suggests that as freshening progresses within the inner  
 264 fjord, the sill can block the export of deep, relatively fresh waters. In 2013, when there was no  
 265 visible difference between interior and exterior casts, the influence of SGD likely did not extend  
 266 below S2. The density differences at depth between 2012 and 2013 further support the hypothesis  
 267 that freshwater is being mixed from the surface downward, as the fjord had both a larger SGD flux  
 268 and a longer time to accumulate freshwater at depth in 2012.



250 FIG. 5. a) MAR SGD flux into SF-SQ in 2012 and 2013. b) The cumulative SGD given in units of gigatonnes  
 251 (Gt). Windows are overlaid during the period of the field campaign in 2012 (red) and 2013 (blue) c) The  
 252 cumulative difference in SGD between 2012 and 2013.

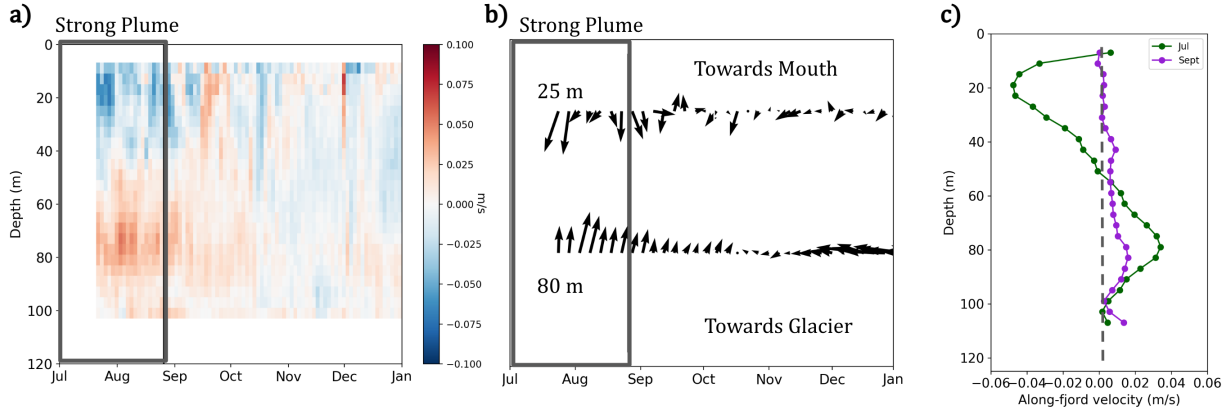
272 *f. Seasonal Change in Circulation*

273 A moored upward-looking ADCP observed fjord circulation for 9 months starting in July 2012,  
 274 and the changes in circulation were consistent with a seasonal response to freshwater input (Fig. 7).  
 275 Since the ADCP is located at a single point in an area of recirculation (Fig 1c; Supplemental Fig.  
 276 6), it provides an incomplete description of the full circulation. However, it remains the best data  
 277 available to characterize the seasonal variation in velocity ~~and~~. Additionally, the depth structure  
 278 of velocity recorded by the ADCP in July is consistent with the snapshot of overturning recorded  
 279 by across-fjord transects (Supplemental Fig 7-10.), indicating that the ADCP measurements are



269 FIG. 6. a) Detrended potential density anomaly for CTD casts in 2012 where the black cast was taken past S2  
 270 in Tasiusaq Fjord. The dashed line is the depth of S2. b) Same as a but for 2013; note that the black cast was  
 271 calculated using an XCTD.

280 correlated with the large-scale fjord circulation. Therefore we separate the ADCP velocity into  
 281 three phases: the plume-driven overturning circulation during the summer, an adjustment period  
 282 in September, and a weaker phase of circulation after October (Fig. 7a). In July, the outflowing  
 283 layer was about 30 m thick and centered around 25 m, while the inflowing layer was 40 m thick  
 284 and centered around the depth of S2, and the deep-basin layer below 100 m had relatively weak  
 285 velocities (Fig. 7c). During this time period, the plume-driven overturning is clear with the upper  
 286 layer (25 m) flowing straight out towards the mouth and the middle layer (75 m) flowing in towards  
 287 the glacier (Fig. 7b). In late August, the estimated SGD flux dropped below  $15 \text{ m}^3/\text{s}$  (10% of  
 288 peak; Fig. 5) and the upper layer was no longer consistently directed oceanward and there was  
 289 intermittent flow reversal. In the middle layer however, the flow remained directed towards the



301 FIG. 7. a) Time series of (2-day running mean) along-fjord velocity from moored ADCP. Negative velocities  
 302 are directed out of the fjord. The time period when SGD is substantial (> 10% of peak) is outlined in black. b)  
 303 Directional plot of the (5-day running mean) along-fjord velocity at the depths 25 m (top) and 75 m (bottom).  
 304 Arrows pointing directly up show flow towards the ~~mouth and away from the~~ glacier. ~~East~~~~West~~ is to the right  
 305 and the along-fjord velocity is defined positive at ~~325~~~~170~~ degrees from North, ~~in line with the main axis of~~  
 306 ~~the fjord at this location~~. c) Vertical profile of along-fjord velocity averaged over the months of July (green) and  
 307 September (purple).

290 glacier, although it was weaker in magnitude and eventually dropped below 0.005 m/s in October.  
 291 During this transition period in September, the along-fjord velocity can be described as weak,  
 292 but steady inflow below 20 m (Fig. 7c). The rapid change in the upper-layer velocity direction  
 293 suggests that the plume-driven overturning is quickly shut down after SGD weakens, but that a  
 294 weaker inflow is still present at depth. This weaker exchange flow could be driven by the density  
 295 gradient between the fjord and S2 (Fig. 6a) that was previously maintained by the plume and  
 296 recirculation. After October, the lower circulation is weak (< 0.005 m/s) and no longer directed  
 297 towards the glacier. The time interval between the plume shut down ( $Q_{sg} < 15 \text{ m}^3/\text{s}$ ) and the shift  
 298 in circulation to weak velocity is approximately 45 days. Although we lack CTD observations in  
 299 the fall, Mernild et al. (2015) show a rapid salinity increase in ~~SF~~~~SQ~~ coincident with the shift  
 300 away from the overturning circulation observed by the ADCP in September.

308 **4. Box Model of Freshwater Storage and Export**

309 We develop a box model to better understand the seasonal variability of fjord circulation and  
310 estimate storage of freshwater. The observations imply that under sustained SGD the fjord freshens  
311 (Fig. 3) and that freshwater is mixed downward throughout the summer (Fig. 6) before eventually  
312 being exported in the fall (Fig. 7). However, we lack measurements to capture this process  
313 continuously and instead rely on observations collected from different years as proxies of different  
314 points in the melt season. A box model enables us to explore the dynamics controlling the seasonal  
315 cycle and quantify timescales for both freshwater storage and export.

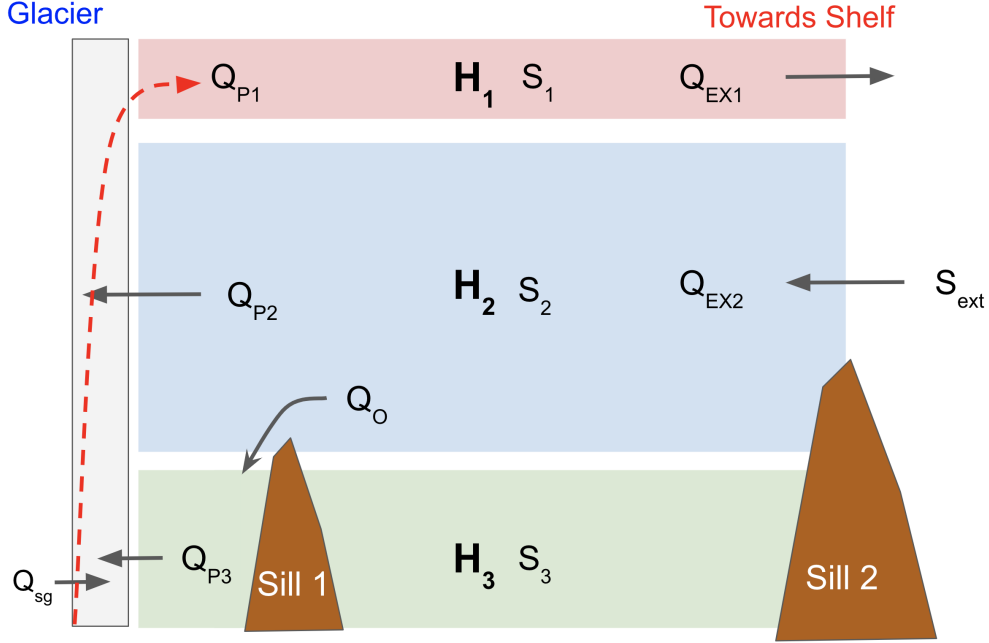
316 The model is similar in style to previous minimal fjord models in that layer thicknesses  
317 and properties evolve according to parameterized exchange with the SGD plume (Zhao et al.  
318 2021) and the ~~continental shelf~~ (Babson et al. 2006; Gillibrand et al. 2013) ~~external fjord basin~~  
319 [\(Tasiusaq, Babson et al. 2006; Gillibrand et al. 2013\)](#). The model is kept as simple as possible  
320 intending to resolve only the first-order dynamics controlling the salinity of the fjord.

321 *a. Box Model Setup*

322 1) MODEL LAYOUT

323 We assume the fjord can be described as a three layer system where the top layer is composed of  
324 outflowing ~~glacially modified~~ [glacially-modified](#) water, the middle layer has inflowing water above  
325 sill height and the [deep-basin](#) layer has water that is isolated in the deep basin by the [sill-sills](#) (Fig.  
326 8). These layers roughly correspond to the observed salinity layers (Fig. 2), and are meant to  
327 represent the overturning circulation within the fjord (Fig. 7c). The boxes are forced by a plume  
328 at the glacier end and can exchange water in and out of the fjord at the sill [end-2](#) (Fig. 8). The  
329 fjord has a total depth  $H$  and surface area  $A$  that is constant with depth. The bottom box represents  
330 the waters below sill depth at all times, and therefore we set and hold fixed  $H_3$ . Since water is  
331 entrained into the plume from this layer, this necessitates the inclusion of an overflow term,  $Q_O$ ,  
332 that represents a flux from the middle layer to the bottom layer. The fjord exterior is assumed to  
333 be composed of water with an average salinity  $S_{ext}$ .

334 Temperature is dynamically passive since density gradients are dominated by salinity, and since  
335 temperature is relatively homogeneous below 15 m we neglect it from the box model. Submarine  
336 melting of the glacier is not included as a freshwater source because it is an order of magnitude



346 FIG. 8. Schematic of the box model comprising an outflowing upper layer, and inflowing middle layer and a  
 347 deep passive layer. Layer thickness and salinity is  $H_j$ , and  $S_j$  respectively where  $j$  denotes the layer. Volume  
 348 flux exchange occurs at the fjord head due to the plume (red) which entrains from the boxes ( $Q_{Pj}$ ) and at the  
 349 outer edge due to fjord-shelf density gradients ( $Q_{EXj}$ ). Sill 1 limits the depth of  $H_1$  and overflow term  $Q_O$  is  
 350 necessary to keep the deep-basin layer volume constant. Sill 2 sets the height of the outflowing layer.

337 smaller than the SGD flux (Table 1) and its omission simplifies the model equations. However in  
 338 fjords that have large concentrations of icebergs such as Ilulissat Isfjord or Sermilik Fjord, SMW  
 339 would have to be included as a freshening term (e.g. Moon et al. 2018, Bearid et al. 2018).  
 340 Furthermore, inclusion of submarine melting in the box model was found to have little impact on  
 341 freshwater storage (Sup. Fig. 11). We wish to keep the model as simple as possible to understand  
 342 the effects of the primary freshwater source (SGD) so we neglect the effects of sea ice, winds,  
 343 icebergs and surface forcing. Lastly, the model does not include mixing between layers explicitly,  
 344 instead mixing is represented through changes in the layer thicknesses which are controlled by the  
 345 balance between the SGD plume and exchange at the mouth.

351 2) PLUME TO FJORD EXCHANGE

352 The effect of SGD is represented through a line plume which entrains ambient water as it rises and  
 353 then outflows into the upper box  $H_1$ . Buoyant plume theory (Jenkins 2011; Straneo and Cenedese  
 354 2015) provides analytical expressions for plume volume fluxes, and the volume of ambient water  
 355 entrained into the plume from the **deep basin** layer is given by

$$Q_{P3} = \alpha^{2/3} (g'_0)^{1/3} w^{2/3} Q_{sg}^{1/3} H_3, \quad (2)$$

356 where  $\alpha$  is the entrainment coefficient,  $g'_0 = g\beta_S S_3$  is the reduced gravity of the SGD relative to  
 357 the **deep basin** layer,  $w$  is the plume width in the across-fjord direction,  $Q_{sg}$  is the SGD and  $H_3$  is  
 358 the thickness of the **deep basin** layer. The volume entrained is therefore determined by the initial  
 359 buoyancy flux ( $g'_0 Q_{sg}$ ) and the height over which the plume rises ( $H_3$ ). The volume entrained from  
 360 the middle layer into the plume is similarly given by

$$Q_{P2} = \alpha^{2/3} (g'_{P2})^{1/3} w^{2/3} (Q_{sg} + Q_{P3})^{1/3} H_2, \quad (3)$$

361 where  $g'_{P2} = g\beta_S (S_2 - S_{P2})$  is the reduced gravity of the plume relative to the middle box and the  
 362 volume flux of the plume entering the middle box has grown to include the entrained water  $Q_{P3}$ .  
 363 The volume flux from the plume into the upper box is then equal to

$$Q_{P1} = Q_{sg} + Q_{P3} + Q_{P2}. \quad (4)$$

364 We also require expressions for the salinity of the plume as it rises. The salinity of the plume as  
 365 it enters the middle box is

$$S_{P2} = \frac{Q_{P3} S_3}{Q_{P3} + Q_{sg}}, \quad (5)$$

366 and the salinity of the plume as it enters box 1 is

$$S_{P1} = \frac{Q_{P3} S_3 + Q_{P2} S_2}{Q_{P3} + Q_{sg} + Q_{P2}}. \quad (6)$$

367 3) EXTERNAL FJORD TO SHELF EXCHANGE

368 The volume flux exchange ~~with the shelf out of the fjord~~ could be parameter-  
 369 ized a number of ways ~~based depending~~ on whether the flow is ~~under externally~~  
 370 ~~forced (e.g., hydraulic control, is geostrophic or is a typical estuarine circulation~~  
 371 ~~(Sutherland et al. 2014; Zhao et al. 2018, 2021). wind forcing)~~ or internally forced which is typical  
 372 ~~for estuarine circulation (Sutherland et al. 2014; Zhao et al. 2018, 2022).~~ Zhao et al. (2021)  
 373 ~~provides scalings for estimating the volume flux at the sill using the density gradient across the~~  
 374 ~~sill for relatively wide (geostrophic transport) or hydraulically controlled fjords.~~ Hydraulic control  
 375 occurs when  $Fr > 1$  at constrictions or sills, ~~but our~~. Our velocity transects show the flow ~~is no~~  
 376 ~~longer critical loses criticality~~ away from the terminus ~~–does not regain it at the sill (Sup. Table 2,~~  
 377 ~~Sup Fig. 13).~~ The importance of geostrophic flow ~~in estuaries~~ can be quantified through the Kelvin  
 378 number ( $Ke = W/L_d$ ), a ratio of the fjord width over the deformation radius  $L_d = c/f$  where  $c$  is  
 379 again the baroclinic wave speed and  $f$  is the Coriolis frequency (Carroll et al. 2017; Jackson et al.  
 380 2018). In ~~SFSQ~~,  $Ke$  is around 1 ~~in the channel~~ suggesting rotational effects are important in the  
 381 wide basin, ~~but throughout the rest of the channel we and that the channel is likely a combination of~~  
 382 ~~vertical and horizontal shear (Valle-Levinson 2008). We~~ found the predicted ~~geostrophic transport~~  
 383 ~~(Zhao et al. 2021) to be much greater than our volume fluxes calculated from hydraulic control~~  
 384 ~~transport (12000 m<sup>3</sup>/s) to overestimate transport from a ship-mounted ADCP transects transect~~  
 385 ~~(Sup Fig 8), suggesting geostrophy was not appropriate in this case~~ 13 (1900-6700 m<sup>3</sup>/s, Sup. Table  
 386 2). However, the predicted geostrophic transport (2600-3600 m<sup>3</sup>/s) was similar to an estimate of  
 387 the gravitational (estuarine) circulation (2200 m<sup>3</sup>/s) lending support for both approaches. We note  
 388 that these two theories are not necessarily incompatible with one another. Ultimately, we choose  
 389 to go with a gravitational parameterization since the primary density gradient we are interested in  
 390 is produced close to the terminus, rather than across the sill. Therefore we ~~parameterize~~ set the  
 391 exchange flow ~~through using~~ a gravitational (estuarine) circulation

$$Q_{EX1} = WU_g \frac{H_s}{2}, \quad (7)$$

392 where  $W$  is the width of the fjord in the channel,  $U_g$  is a scalar velocity for the gravitational  
 393 circulation and  $H_s/2$  is half the sill depth and a scale height associated with the gravitational

394 circulation to turn it into a volume flux. Note that we are solving for the volume flux and not for  
 395 the layer velocity, since  $U_g$  is a scalar velocity not the velocity in a specific layer. In this way, a thin  
 396 layer should be physically associated with a concentrated flux (faster velocity) and a larger layer  
 397 should be associated with a diffuse flux (slower velocity).

398 While gravitational circulation is often dominant in shallower estuaries, we believe it is still  
 399 appropriate for some glacial fjords despite their relatively large depths due to the vigorous mixing  
 400 occurring within the plume system, along sidewalls or at sills. An estimate for the strength of  
 401 the gravitational circulation can be derived assuming a balance between the baroclinic pressure  
 402 gradient and friction (Geyer and MacCready 2014)

$$U_g = \frac{g\beta_s H_{12} \bar{S}_x}{r}, \quad (8)$$

403 where  $\bar{S}$  is the vertically-averaged salinity over the first two layers, the subscript  $x$  denotes an along-  
 404 fjord gradient and  $1/r$  is a frictional time scale. Equation 8 is a modified gravitational circulation  
 405 where the classical mixing time scale  $H^2/K_m$  has been replaced by a frictional time scale  $1/r$  due  
 406 to uncertainty in the source of mixing. The average along-fjord salinity gradient can be rewritten:

$$\begin{aligned} \bar{S}_x &= \frac{1}{L} \left( S_{ext} - \bar{S} \right), \\ &= \frac{1}{L} \left( S_{ext} + \frac{H_1}{H_{12}} (S_2 - S_1) - S_2 \right). \end{aligned} \quad (9)$$

407 where  $L$  is the along fjord length scale, which we have chosen to be the distance from the glacier  
 408 to the shelf.

409 Combining equations 7, 8, and 9 gives:

$$\begin{aligned} Q_{EX1} &= \frac{\frac{g\beta_s H_{12} H_s W}{2r}}{\frac{g\beta_s H_{12} H_s W}{2Lr}} \left( S_{ext} + \frac{H_1}{H_{12}} (S_2 - S_1) - S_2 \right), \\ &= \frac{\Gamma_{EX}}{r} \Delta \bar{S}. \end{aligned} \quad (10)$$

410 with the salinity gradient ( $\Delta\bar{S}$ ), friction ( $r$ ) and fjord geometry ( $\Gamma_{EX}$ ) controlling exchange with  
 411 the ~~shelfout of the fjord~~. The inflowing exchange flow term is defined overall from conservation  
 412 of volume within the fjord to be

$$Q_{EX2} = Q_{EX1} + Q_{sg} + Q_O. \quad (11)$$

413 4) CONSERVATION EQUATIONS

414 Using the Boussinesq approximation, we neglect variations in density and approximate mass  
 415 conservation with volume conservation. The conservation of volume for each of the boxes is given  
 416 by the equations

$$A \frac{dH_1}{dt} = Q_{P1} - Q_{EX1}, \quad (12)$$

$$A \frac{dH_2}{dt} = -Q_{P2} + Q_{EX2}, \quad (13)$$

$$A \frac{dH_3}{dt} = -Q_{P3} + Q_O = 0, \quad (14)$$

417 where the choice  $Q_O = Q_{P3}$  ensures the thickness of the deep box does not change. After  
 418 substituting the volume conservation equations (12,13,14) into salinity conservation equations we  
 419 arrive at the simplified salinity equations:

$$AH_1 \frac{dS_1}{dt} = Q_{P1}(S_{P1} - S_1), \quad (15)$$

$$AH_2 \frac{dS_2}{dt} = Q_{EX2}(S_{ext} - S_2), \quad (16)$$

$$AH_3 \frac{dS_3}{dt} = Q_O(S_{ext} - S_3). \quad (17)$$

420 5) INITIAL CONDITIONS AND FORCING

421 The model is initially set up to resemble ~~SF-SQ~~ in the spring before the melt season. We assume  
 422 that each year the fjord is completely flushed of freshwater and replenished with shelf waters

423 composed of a single water mass. This assumption is supported by salinity observations of the  
 424 ~~deep-basin~~ layer being the same in both 2012 and 2013. Therefore, we initially set  $S_{ext} = S_1 = S_2 =$   
 425  $S_3 = 33.57$  g/kg such that at the start of the melt season the box model is constant in salinity. In the  
 426 absence of submarine melting, and provided that  $S_{ext}$  is also constant in time (an assumption we  
 427 make for these simple simulations), we then have  $S_2 = S_3 = S_{ext}$  throughout the simulation. This  
 428 choice simplifies the vertically averaged salinity to be

$$\bar{S} = S_{ext} - \frac{H_1}{H_{12}}(S_{ext} - S_1). \quad (18)$$

429 While this model includes a constant external salinity and constant friction coefficient, versions  
 430 of the model with time-varying constants gave qualitatively similar results (Sup. Fig 14). The  
 431 layer thicknesses are initially set to  $H_1 = 2$  m,  $H_2 = 98$  m, and  $H_3 = 50$  m, which is the height of  
 432 sill 1. A minimum thickness of 2 m is required for the top two layers to keep the model stable and  
 433 ensure that the model always has all three layers present. The box model geometry is chosen to be  
 434 as close as possible to ~~SF-SQ~~ with  $A = 6.26 \times 10^7$  m<sup>2</sup>,  $W = 2$  km,  $H_s/2 = 40$  m and  $L = 60$  km.  
 435 For the plume parameters,  $\alpha = 0.13$ ,  $w = 90$  m, and  $\beta_S = 0.75 \times 10^{-3}$  kg/g (Jackson et al. 2017).  
 436 The friction coefficient  $r = 0.0012$  1/s was chosen because it produced the best model fit with the  
 437 observations. It is hard to compare this friction coefficient with observations, however comparison  
 438 against a close analog, the diffusivity mixing time scale  $H_{12}^2/K_m$ , suggest the value of the coefficient  
 439 is high (see Supplemental). The relatively high friction may be seen as compensating for the lack  
 440 of recirculation in the box model.

441 The model is forced with SGD taken from the regional climate model MAR (Fig. 5; Mankoff  
 442 et al. (2020)) and we assume a 15% uncertainty (Mankoff et al. 2020). The model is solved by  
 443 stepping through the conservation equations with a Backwards Implicit Euler scheme using a 0.1  
 444 day timestep. The model is run from day 70 to day 365 in each of 2012 and 2013.

#### 445 b. Model Results

446 We start with the box model's seasonal evolution and then compare the predicted salinity and  
 447 salinity trends with observations. As SGD enters the fjord, the exchange ~~with the shelf out of the~~  
 448 ~~fjord~~ is initially weak and so the top layer thickens (Fig. 9a).  $H_1$  thickens earlier in 2012 than 2013  
 449 since SGD enters the fjord earlier, but both reach a maximum thickness of about 70 m. The salinity

450 in the upper layer decreases (Fig. 9b) as freshwater is not sufficiently exported. The freshening of  
 451 the upper layer starts earlier in 2012, but both years reach a minimum in salinity near day 218. As  
 452  $Q_{sg}$  weakens at the end of summer then the average salinity in the plume grows (Eq. 6) and  $S_1$   
 453 starts to level off. Since the reduction in  $Q_{sg}$  occurs at a similar time in 2012 and 2013, salinity  
 454 minimums in  $S_1$  occur at similar times in both years.

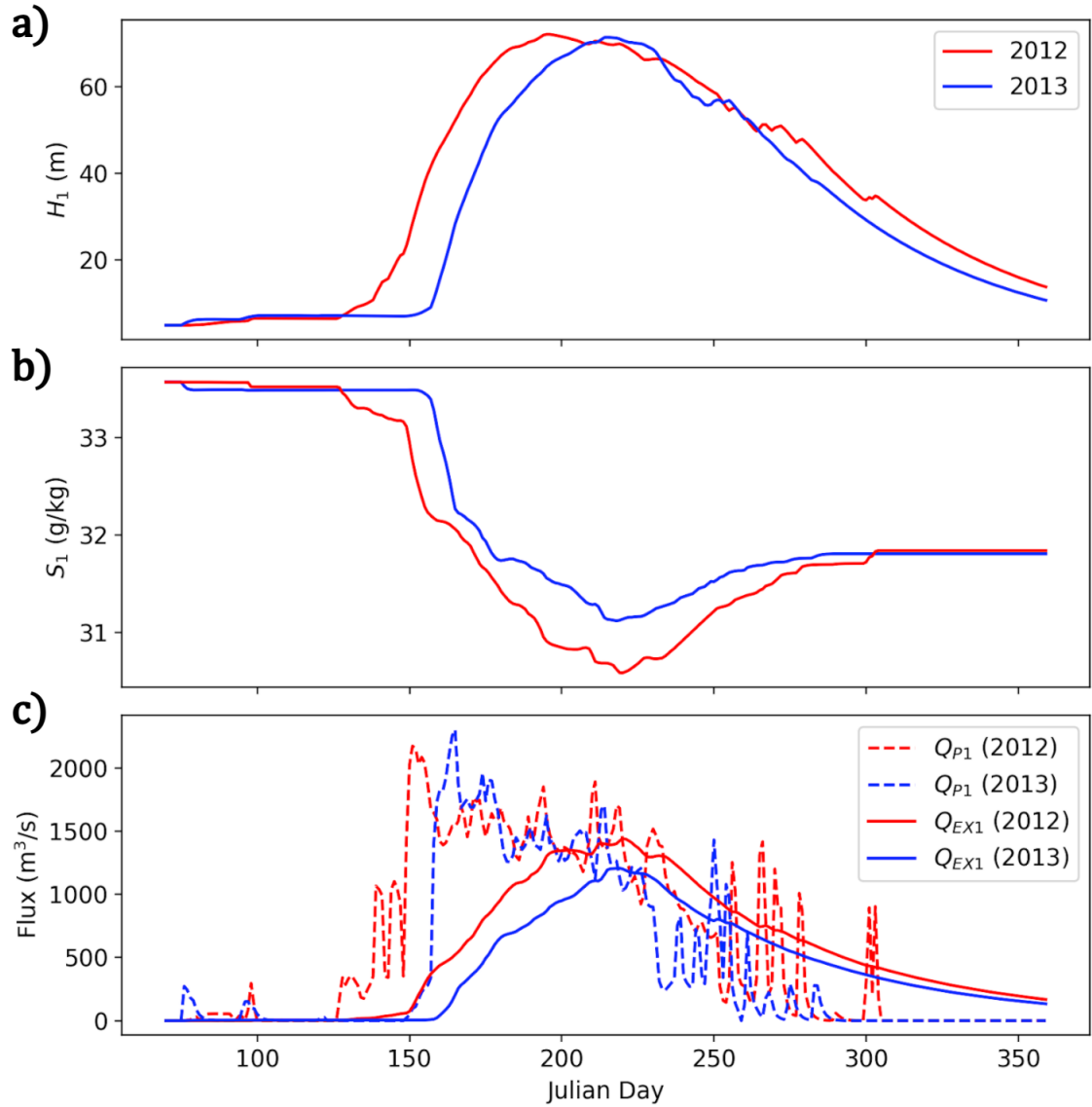
455 As the upper layer gets thicker, the plume has less distance to rise and so less volume is entrained  
 456 by the plume, decreasing  $Q_{P1}$  (Fig. 9c). At the same time, the changes in  $H_1$  and  $S_1$  increase the  
 457 density gradient between the fjord and ~~shelf~~external fjord basin resulting in a higher exchange flow  
 458  $Q_{EX1}$ .  $H_1$  increases until the exchange flow is greater than the inflow from the plume. Ultimately  
 459 however,  $Q_{EX1}$  overtakes  $Q_{P1}$  only when  $Q_{sg}$  decreases and the plume shuts down. Since the  
 460 crossing point is tied to  $Q_{sg}$ , it also occurs at a similar time in both years.

461 When  $Q_{EX1}$  overtakes  $Q_{P1}$  the fjord starts to ~~export~~net export the freshwater that was stored  
 462 during the melt season Fig. 9c. We can estimate a timescale for this export as the time taken to  
 463 exchange all water in the upper layer if the exchange is maintained at its maximum value:

$$\tau_{export} = \frac{AH_1(t_{min})}{Q_{EX1}(t_{min})}, \quad (19)$$

464 where  $t_{min}$  is the time when the salinity is minimized and  $Q_{sg}$  starts to fall off. In 2012 and  
 465 2013,  $\tau_{export} = 48$  and 57 days, respectively, which is similar to the 45 day adjustment timescale  
 466 estimated from changes in the baroclinic circulation in 2012 (Fig. 7).

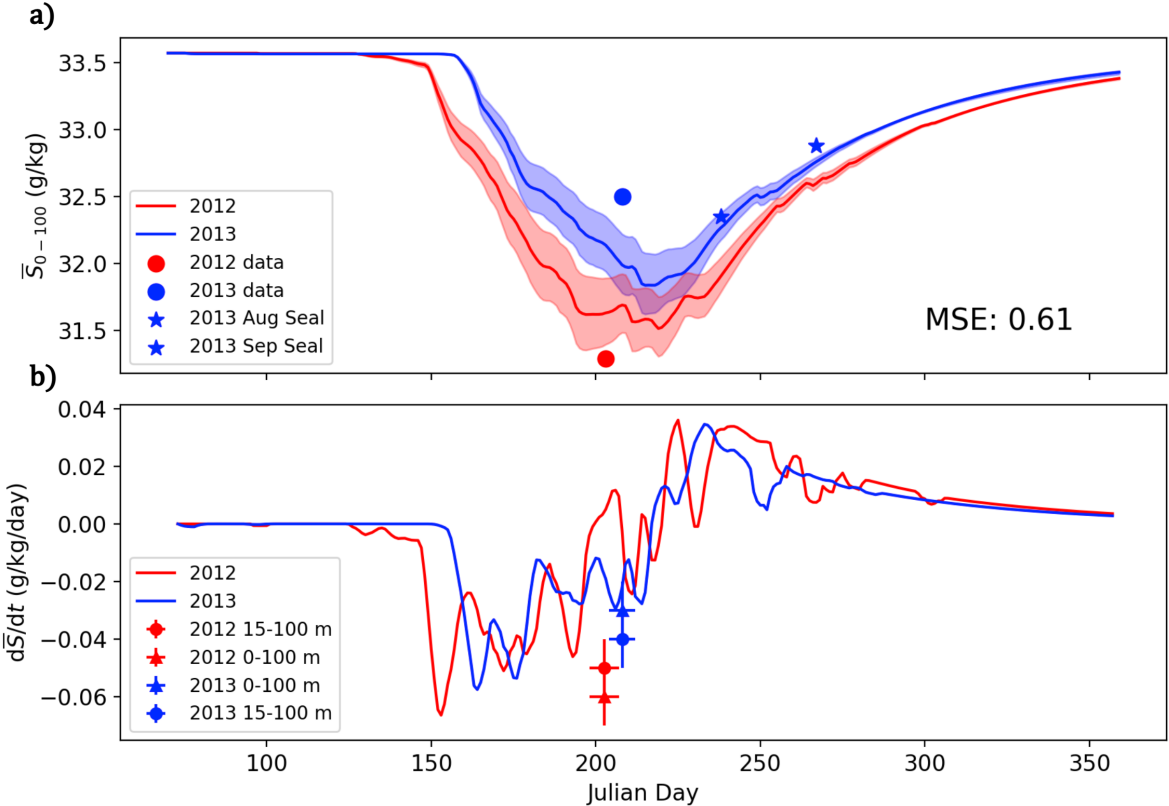
470 The box model results compare reasonably well with the  $\bar{S}$  measurements from CTD casts  
 471 collected in 2012 and 2013, with a mean square error (MSE) of 0.61 g/kg that is reduced after  
 472 taking into account the uncertainty in  $Q_{sg}$  (Fig. 10a). The model also predicts an increase in  
 473 vertically averaged salinity after the plume shuts off that is consistent with the seal observations  
 474 from Mernild et al. (2015). The modeled magnitude of salinity trend early in the season matches  
 475 the magnitude of the observations, but suggest that the magnitude of  $d\bar{S}/dt$  (Fig. 10b) decreases  
 476 over summer. Taken as whole, the comparisons against observations suggest the box model  
 477 does a reasonable job of capturing the observed salinity properties given the model's simplicity.  
 478 Potentially, the model needs a greater sensitivity to  $Q_{sg}$ , since  $\bar{S}$  is underestimated in 2012 and  
 479 overestimated in 2013.



467 FIG. 9. a) Box model  $H_1$  for 2012 (red) and 2013 (blue) as a function of Julian day. b) same as a, but for  $S_1$ .  
 468 c) Volume fluxes in and out of the top box with dashed lines for the plume fluxes in and solid lines for exchange  
 469 flow fluxes out.

487 *c. Freshwater Export*

488 The combined mean salinity of a layer  $H_{fw}$  of pure freshwater and a layer  $H_{12} - H_{fw}$  of water  
 489 with salinity  $S_{ext}$  is



480 FIG. 10. a) Comparison of the observed vertically averaged salinity ( $\bar{S}$ ) from 0 to 100 m from both the field  
 481 campaigns and Mernild et al. (2015) seal data against the box model vertically averaged salinity. The shading  
 482 represents the uncertainty due to SGD flux. b) The derivative of  $\bar{S}$  from the box model compared against the  
 483 observed salinity trends (Fig. 3). The circles are the salinity trend from 15 - 100 m (Fig. 3) while the triangles  
 484 are the observed trend from 0 - 100 m. The horizontal error bars represent the length of the field campaign and  
 485 vertical error bars represent the uncertainty in the salinity trend. Note the box model does not contain any surface  
 486 forcing.

$$\bar{S}_{fw} = \frac{H_{fw}S_{fw} + (H_{12} - H_{fw})S_{ext}}{H_{12}}, \quad (20)$$

490 and therefore we could define the pure freshwater volume in the fjord by  $V_{fw} = AH_{fw}$ , assuming  
 491 that there is no freshwater below the inner sill. The mean salinity in Eq. 20 is equivalent to  $\bar{S}$  (Eq.  
 492 18) and so the net freshwater accumulation or export can be be expressed as

$$\frac{dV_{fw}}{dt} = A \frac{dH_{fw}}{dt} = -H_{12}A \frac{d\bar{S}}{dt} \frac{1}{S_{ext}}, \quad (21)$$

493 after rearranging Eq. 20 and taking the derivative. Additionally, since we know the freshwater  
 494 fluxes into the fjord ( $Q_{sg}$ ) we can solve for the freshwater flux out of the fjord  $Q_{fw}$  through the  
 495 relation

$$Q_{fw} = Q_{sg} - \frac{dV_{fw}}{dt}. \quad (22)$$

496 As seen in the box model salinity, the fjord begins to accumulate freshwater once  $Q_{sg}$  is non-zero  
 497 in early summer (Fig. 11a), because the exchange ~~with the shelf out of the fjord~~ is insufficient  
 498 to balance the plume fluxes (Fig. 9c, 11b). Freshwater continues to accumulate until it reaches  
 499 a maximum at 0.3 - 0.4 Gt around day 218 in both 2012 and 2013. Beyond this,  $Q_{sg}$  decreases  
 500 and the export of freshwater ~~to the shelf between fjord basins~~ exceeds freshwater input, so that the  
 501 freshwater volume in the fjord decays exponentially through the fall (Fig. 11a-b). The peak of  $Q_{fw}$   
 502 is smaller than the peak magnitude of  $Q_{sg}$  because the freshwater flux is distributed over a longer  
 503 time period. In both years, the peak freshwater fluxes from the fjord are offset from SGD input by  
 504 about a month (Fig. 11b). The ratio of freshwater stored,  $R = 1 - Q_{fw}/Q_{sg}$ , shows a roughly linear  
 505 decrease in freshwater storage with most freshwater stored early in the season, and most exported  
 506 late in the season (Fig. 11c).

#### 511 *d. Scaling for freshwater storage*

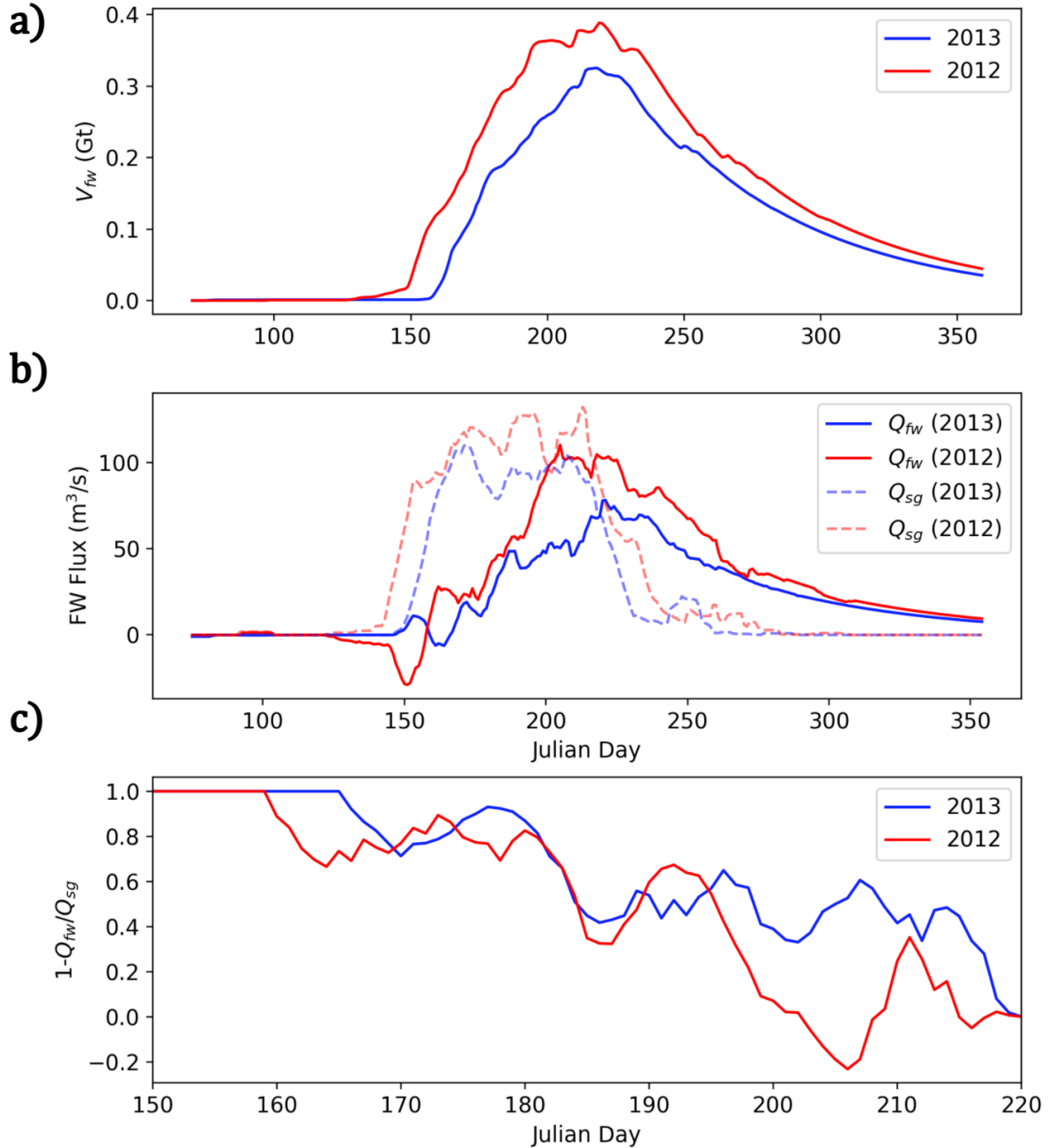
512 We can generalize the results of the box model to other fjord systems by examining the factors  
 513 controlling the boundary volume fluxes which set the fjord freshwater content. First, we scale the  
 514 salinity gradient as

$$\bar{S}_x = \frac{V_{fw}}{V_f + V_{fw}} \frac{S_0}{L_S}, \quad (23)$$

515 where  $V_{fw}$  is the volume of freshwater inside the fjord,  $V_f = HLW$  is the volume of the fjord,  $S_0$   
 516 is a reference salinity and  $L_S$  is the length scale of the salinity gradient, which is not necessarily  
 517 the same as the length scale of the fjord. Noting that  $V_f \gg V_{fw}$ , we end up with a scaling for the  
 518 exchange flow from Eq. 10 as

$$Q_{ex} = C_{out} \times \frac{H_s V_{fw}}{2 L L_S r}, \quad (24)$$

519 where  $C_{out} = g \beta_S S_0$  includes all the constants which vary little from fjord to fjord.



507     Fig. 11. a) The volume of freshwater ( $V_{fw}$ ) stored in the box model for 2012 (red) and 2013 (blue) as a  
 508     function of Julian day. b) Freshwater export ( $Q_{fw}$ ) from Eq. 22 and SGD ( $Q_{sg}$ ) in the box model. The a 10-day  
 509     running mean has been applied to smooth the signal. c) The fraction of SGD that was stored in the fjord during  
 510     the time period when the plume was active.

520 Similarly the plume flux can be approximated from Eq. 2 as

$$Q_p = C_{in} \times Q_{sg}^{1/3} H^* + Q_{sg} + Q_{smw}, \quad (25)$$

521 where  $C_{in} = \alpha^{2/3} g'^{1/3} w^{2/3}$  is a constant,  $H^* = H_{gl} - H_s/2$  is the height the plume rises before it  
 522 enters the top box, and  $Q_{smw}$  is the submarine meltwater contribution. Noting that  $Q_{smw}$  and  $Q_{sg}$   
 523 are much smaller than the first term (e.g. Mankoff et al. 2016), the ratio of export to storage can be  
 524 written as

$$R_{stor} = \frac{C_{out} V_{fw} \delta}{C_{in} Q_{sg}^{1/3} L L_{sr}}, \quad (26)$$

525 where  $\delta$  is the height of the outflowing layer ( $H_s/2$ ) over the height of the rising plume ( $H^*$ );  
 526 analogous to the height of the sill over the height of the grounding line. If the grounding line is  
 527 the same depth as the sill then  $\delta=1$ , while realistic examples are  $\delta=0.18$  for Ilulissat Isfjord (IL),  
 528 0.36 for ~~Sarqardleq Fjord~~ (SF) ~~Saqqarleq~~ (SQ) and 0.73 for Sermilik ~~Fjord~~ (SK) ~~(SM)~~. From Eq 26  
 529 it is clear that  $\delta$  is an important parameter controlling freshwater residence time, consistent with  
 530 Carroll et al. (2017). Additionally, increasing the length of the fjord and the density gradient length  
 531 scale reduce the exchange flow strength, although for larger systems this increase in storage is  
 532 likely compensated by a larger total freshwater content ( $V_{fw}$ ) which increases the density gradient.  
 533 If friction is dominated by bottom dissipation, then  $r$  will be smaller in deeper fjords, but if  $r$  is  
 534 primarily determined by sidewall dissipation or mixing near the plume it might take a similar value  
 535 from system to system.

536 We can evaluate how  $V_{fw}$  compares across fjord systems under steady state. Initially, the stored  
 537 freshwater will start out small and all glacial fjords should be in a position where  $R_{stor} < 1$ . However  
 538 as  $V_{fw}$  increases, a steady state regime will be reached when  $R_{stor} = 1$ . Using representative values  
 539 (Table d): we set  $R_{stor} = 1$  and get a  $V_{fw}$  of 1.9, 0.20, and 2.5 ( $10^9 \text{ m}^3$ ) for ~~SK~~, ~~SF~~ ~~SM~~, ~~SQ~~ and IL,  
 540 respectively, indicating IL will store the most freshwater before exchange is efficient at removing  
 541 it. However, as a proportion of fjord volume these are 0.004, 0.03, and 0.008 for ~~SK~~, ~~SF~~ ~~SM~~,  
 542 ~~SQ~~, and IL which indicates we should expect the greatest changes in mean salinity to occur in  
 543 ~~SF~~ ~~SQ~~. Based on Eq. 26, we see that ~~SF~~ ~~SQ~~ might be uniquely placed to observe large freshening  
 544 because it is relatively small and has a moderate sill height compared to grounding line depth. For  
 545 other systems, such as ~~SK~~ ~~SM~~, the combination of a deep sill and large fjord volume may limit the

546 observed freshening. With a known rate of freshwater input (eg,  $Q_{smw}$  or  $Q_{sg}$ ), this threshold  $V_{fw}$   
 547 could be turned into a residence time. However, these results are based on the assumption that  
 548 fjord circulation can be described as a gravitational circulation. The exchange of other glacial fjord  
 549 systems might be primarily wind-driven, geostrophic or hydraulically controlled (e.g. Jackson et al.  
 550 2014; Schaffer et al. 2020; Zhao et al. 2021) and so care should be taken in choice of the exchange  
 551 flow parameterization. Lastly, for systems with significant iceberg cover, we expect iceberg melt  
 552 to significantly impact the freshwater budget such that it should be accounted for in the box model  
 553 Moon et al. (2018); Davison et al. (2020).

Fjord	$Q_{sg}$	$L$	$L_s$	$V_f$	$\delta = H_s/2H^*$
Sermilik	1350 m <sup>3</sup> /s	90 km	90 km	$5 \times 10^{11}$ m <sup>3</sup>	0.73
<del>Sarcqardleq</del> <del>Saqqarleq</del>	125 m <sup>3</sup> /s	16 km	60 km	$7 \times 10^9$ m <sup>3</sup>	0.36
Ilulissat	1750 m <sup>3</sup> /s	50 km	50 km	$3 \times 10^{11}$ m <sup>3</sup>	0.18

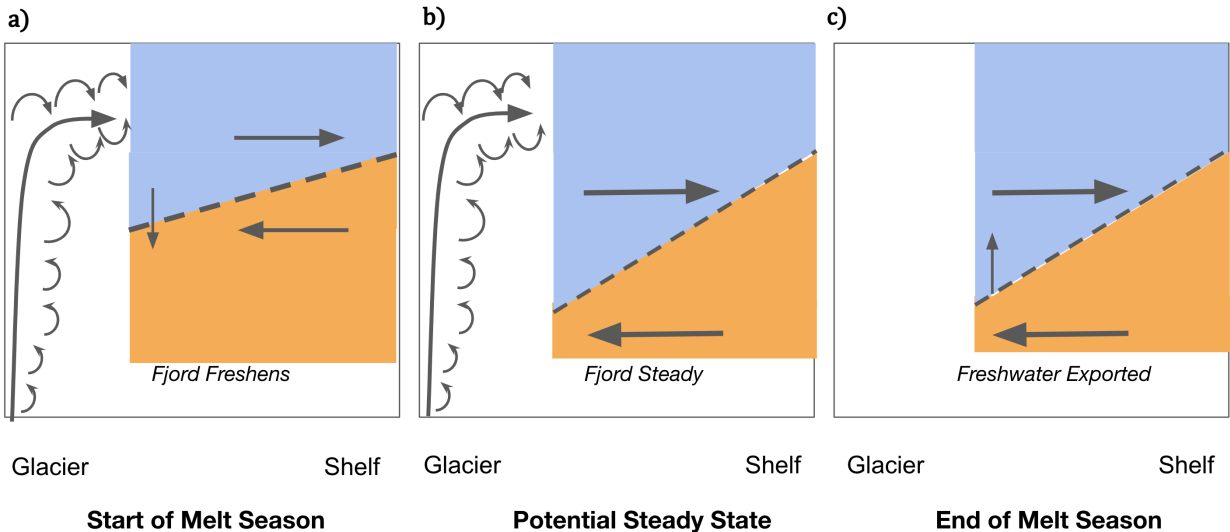
544 TABLE 2. Table of values used in the exchange flow scaling for three fjord systems.  $Q_{sg}$  is the average SGD in  
 545 July in 2012 and 2013 (Mankoff et al. 2020). For Sermilik and Ilulissat ~~Fjords~~ we assume  $L = L_s$  because these  
 546 systems connect directly with the shelf.

## 557 5. Discussion

### 558 a. Mechanisms driving freshwater storage

559 We observe that the mean salinity of ~~SF-SQ~~ decreases during the melt season due to the ~~net~~  
 560 accumulation of freshwater. We propose that this process occurs primarily through vertical mixing  
 561 of SGD. Initially, the density-driven exchange ~~with the shelf out of the fjord~~ is insufficient at  
 562 removing freshwater stored near the head, but as the fjord freshens, the exchange flow increases  
 563 until either the plume shuts off or the fjord reaches steady state. In this section, we discuss these  
 564 steps in more detail and discuss the possible physical processes contributing to freshwater storage.

565 The hydrographic observations indicate that the region close to the glacier (< 6 km from the  
 566 terminus) was accumulating freshwater during the field seasons (Fig. 3) and that the freshening  
 567 occurred from the surface downward. While submarine melting of glaciers, especially in larger  
 568 fjords, provides a freshening source at depth, we identify SGD as the primary freshwater being  
 569 stored. This finding is consistent with independent estimates of freshwater flux into the fjord as



584     Fig. 12. Schematic of the freshwater storage process. The first panel represents the start of the melt season  
 585     with mixing near the head of the fjord deepening the pycnocline and relatively weak exchange flow. The middle  
 586     panel represents a potential steady state that could be reached during the melt season between exchange **with the**  
 587     **shelf** and mixing within the fjord. The third panel represents the end of the melt season or when mixing tied to  
 588     the buoyancy-driven circulation weakens and exchange **with the shelf** is strong.

570     Wagner et al. (2019) estimated a combined calving and SMW flux of 0.5 Gt/yr during summer  
 571     compared to our MAR-estimated SGD flux of 3.5 - 4.4 Gt/yr during summer.

572     Using our box model we explored the balance between plume-driven freshwater storage and  
 573     density-driven freshwater export **between fjord basins**. Early in the melt season, the exchange  
 574     **with the shelf out of the fjord** is weak and freshwater from the jet is mixed vertically (Fig. 12a).  
 575     This process deepens the pycnocline within the fjord, akin to  $H_1$  increasing in the model, and  
 576     is consistent with observed stratification and density profiles of the fjord (Figs. 2, 6). As the  
 577     pycnocline deepens, the along-fjord density gradient between the fjord and the shelf increases until  
 578     a crossing point is reached between the tendency for storage and export (Fig. 12b). After the  
 579     plume shuts down, freshwater is no longer accumulated and the fjord adjusts through exchange  
 580     with the **shelf external fjord basin** over the next 45 days (Fig. 12c). **In reality, the along-fjord**  
 581     **density gradient is non-linear in space with the majority of the isopycnal gradients occurring close**  
 582     **to the glacier (Mankoff et al. 2016), and mixing in the rest of the fjord likely relatively weak, but**  
 583     **not negligible (Bendtsen et al. 2021).**

589 In our box model, the mixing of freshwater between layers is not represented explicitly and  
590 instead is included in the ~~shelf~~-exchange parameterization through the frictional time scale  $1/r$ .  
591 Although the friction appears physically consistent with shear-driven mixing from the jet (see  
592 Supplemental), other possible sources of mixing which could be represented include dissipation  
593 along the walls of the fjord or in the lee of a sill. These mixing processes are common in non-glacial  
594 fjords (Klymak and Gregg 2004; Staalstrøm et al. 2015) and along sinuous submarine canyons  
595 (Wain et al. 2013), and will be intensified in the presence of recirculation. Additionally, small scale  
596 mixing from the submarine melting of ice outside of the plume would enhance the background  
597 diffusivity, and future field campaigns should be designed to estimate the energy budgets of these  
598 systems.

599 The parameterization could further be improved by representing recirculation which likely acts  
600 to increase the residence time of freshwater in the fjord. Recirculation gyres driven by plumes are  
601 found in both observations and models to exist near termini in fjord (Carroll et al. 2017; Slater  
602 et al. 2018; Zhao et al. 2021) and large scale recirculations in glacial fjords are connected to glacial  
603 melt-rates and overturning strength (Zhao et al. 2022). The strong recirculation cell in ~~SF-SQ~~ can  
604 potentially contribute to freshwater storage by redirecting SGD away from the export and back into  
605 the plume. Although only a snapshot, ADCP transects across the fjord indicate the volume flux in  
606 the recirculation gyre was substantially higher than in the main channel and approximately 50% of  
607 the main outflow was redirected back towards the plume in 2013.

608 We therefore propose the stratification of the fjord increased during the summer, in part due to  
609 vertical mixing of freshwater. Glacial fjord plumes are energetic and turbulent (Podolskiy et al.  
610 2021), and shear-driven mixing from buoyant jets can take freshwater at the surface (or within the  
611 plume itself) and mix it down below the primary export depth. Recently Bendtsen et al. (2021)  
612 found that turbulent mixing rates close to the terminus of Store Gletscher were 100 times higher  
613 than mixing rates in the rest of the fjord. Additionally, De Andrés et al. (2020) showed that in  
614 2012 the hydrographic properties of the plume-turned-jet were significantly diluted within a few  
615 hundred meters of the terminus indicating that there was additional entrainment and mixing by  
616 the jet outflow. Velocity transects across ~~SF-SQ~~ (Sup. Figs. 6-10), show that the Froude number  
617  $Fr = U/c$ , a ratio of the advective speed  $U$  over baroclinic wave speed  $c$ , is greater than 1 in the

618 core of the outflowing jet indicating that the jet was an inertial-driven flow susceptible to strong  
619 shear-driven mixing.

620 Freshwater storage has also been observed in a glacial fjord in LeConte, Alaska due to the  
621 outflow plume impinging on the sill and being redirected back towards the glacier (Hager et al.  
622 2022). In that study, a reflux coefficient (Cokelet and Stewart 1985; MacCready et al. 2021) is  
623 calculated which quantifies the amount of export that is mixed vertically back towards the glacier.  
624 In a more generic box model than the one we have presented, a reflux coefficient that is a function  
625 of  $Q_{sg}$  could be added to the ~~shelf-exchange~~-fjord-exchange parameterization. Tidal flow over  
626 the sill is responsible for the intense mixing which leads to the observed freshwater storage in  
627 Godthåbsfjord Mortensen et al. (2011, 2014). Another potential source of mixing includes internal  
628 waves which can be generated by the plume when it impinges on the pycnocline or from tidal flow  
629 over the sill (Ezhova et al. 2016, 2017; Mortensen et al. 2014; Stuart-Lee et al. 2021). Therefore,  
630 sills and regions close to the terminus are likely mixing "hot spots" that are elevated by SGD  
631 plumes and buoyancy-driven circulation (Bendtsen et al. 2021). Lastly, the interior stratification  
632 of the fjord could increase due to the compression of isopycnals with no significant interior mixing  
633 taking place. In this scenario, the isopycnal layer corresponding to the neutral buoyancy depth of  
634 the plume thickens and the isopycnals below and on top of the neutral buoyancy depth get closer  
635 together. However, if this was the dominant mechanism of observed freshening, then the profiles  
636 would overlap in TS space in contrast to our observations, which indicate mixing with SGD and  
637 SMW (Fig. 4).

638 *b. Delayed Freshwater Export*

639 In ocean circulation models that include Greenland Ice Sheet freshwater forcing, the effects of  
640 freshwater storage within glacial fjords should be included as the potential lag can be significant.  
641 The lag in peak freshwater export, or freshwater residence time, determined from the box model  
642 in ~~SF-SQ~~ is about a month. Our estimated timescale of stored freshwater export is faster than in  
643 nearby Ameralik fjord (Stuart-Lee et al. 2021) and Godthåbsfjord (Mortensen et al. 2018), but  
644 these glacial fjords have strong tidal mixing and are primarily renewed by dense coastal overflows  
645 in the winter. However, our timescale of stored freshwater export is similar to the timescale of  
646 destratification that occurs in the fall in LeConte, Alaska (Hager et al. 2022).

647 It is clear that the lag in freshwater export will be determined by the relationship between  
648 exchange at the mouth  $Q_E$  and the volume flux from the plume  $Q_P$  as our scaling showed (Eq. 26).  
649 In a system where  $Q_E$  is primarily driven by shelf-forcing (e.g. along-shore winds, eddies, coastal  
650 trapped waves) then  $Q_E$  will be independent of  $Q_P$  and freshwater storage will be set by whether  
651 the shelf forcing acts to enhance or reverse the buoyancy-driven flow (Giddings and MacCready  
652 2017). If however,  $Q_E$  is driven by buoyancy forcing from the glacier, then its value at the mouth  
653 will be sensitive to the amount of reflux or recirculation which occurs within the fjord both of  
654 which can act to increase freshwater storage. These volume fluxes will also be influenced by fjord  
655 geometry. For example, fjords that are narrow and have shallow sills will limit  $Q_E$  resulting in a  
656 larger delay of freshwater export (Zhao et al. 2021). Given the sensitivity of fjord-shelf exchange  
657 to a number of parameters (e.g. tides, winds, iceberg presence, fjord geometry), continental-wide  
658 estimates of freshwater export delay will need to be informed by observations of both hydrography  
659 and bathymetry from within a large number of ~~Greenlandic~~ ~~Greenland's~~ glacial fjords (Straneo  
660 et al. 2019).

### 661 *c. Applicability to other fjord systems*

662 Due to several factors such as fjord size and the presence of a single oceanic water mass, it is  
663 easier to detect freshwater storage in ~~SF~~ ~~SQ~~ than in other glacial fjords. As shown with Eq. 26, the  
664 volumes of larger glacial fjords such as Sermilik ~~Fjord~~ or Ilulissat Icefjord reduce the magnitude  
665 of observable salinity trends despite greater freshwater fluxes. However, Stuart-Lee et al. (2021)  
666 observed freshwater storage and delayed export occurring in Ameralik, a land-terminating glacial  
667 fjord in West Greenland. In that study they attributed the freshwater storage to intense tidal mixing  
668 at the sill which drew down freshwater from the surface and increased fjord stratification during  
669 the summer and into the fall. This process could also be occurring in ~~SF~~ ~~SQ~~ and future work  
670 should aim to quantify the contribution of tidal mixing at the sill versus mixing induced by the  
671 plume/jet. We attribute the mixing primarily to physical processes linked with the jet because we  
672 observe freshening first near the terminus and then at S2. However, the two mixing processes are  
673 likely working together to increase the fraction of freshwater that is stored.

674 The processes that led to rapid freshening in ~~SF~~ ~~SQ~~, including turbulent plumes and glacier-wide  
675 recirculation, will be active in all of Greenland's major glacial fjords since they are driven by

676 SGD. Making equivalent observations to those in ~~SF-SQ~~ at large glacier-fjord systems is extremely  
677 challenging due to mobile and thick ice ~~melange~~mélange, but the downsloping isopycnals observed  
678 near the heads of some glacial fjords (Gladish et al. 2014; Jackson and Straneo 2016; Beaird et al.  
679 2015) could be evidence of a vigorous near-terminous circulation. Experiments with additional  
680 endmembers, such as noble gases or oxygen, which can be used as meltwater tracers, are needed  
681 to confirm the late departure of freshwater in other systems (Beaird et al. 2015, 2017, 2018).

## 682 6. Conclusion

683 Glacial fjord circulation and properties are often described as bi-modal with plume-driven circu-  
684 lation and strong stratification in the summer and a shelf-driven circulation and weak stratification  
685 in the winter. This viewpoint overlooks the potentially significant subseasonal variability within  
686 fjords and the potential for transient storage of ice sheet freshwater. We find evidence that during  
687 the summer, freshwater is stored within ~~Sarqardleq Fjord~~Saqqarleq, a mid-sized glacial fjord in  
688 west Greenland, resulting in non-steady mean salinity during the melt season. Specifically, obser-  
689 vations of salinity collected in ~~SF-SQ~~ show a freshening trend of 0.05 g/kg/day and 0.04 g/kg/day  
690 in 2012 and 2013 respectively . The observations suggest that vertical mixing of SGD increases  
691 stratification and freshwater content within the fjord when the plume is active. We developed a box  
692 model that is forced by SGD at its glacial boundary and a density-driven exchange with ~~the shelf at~~  
693 ~~the ocean at its sill~~ boundary. Competition between these boundary conditions determines whether  
694 freshwater is being stored or removed from the fjord. The box model indicates that glacial fjords  
695 with intense mixing are inefficient at removing freshwater, resulting in a lag of 25-30 days between  
696 the peak SGD entering the fjord and the freshwater export from the fjord. Future work should aim  
697 to identify this process in larger glacial fjords and quantify the interior mixing that redistributes  
698 freshwater. Our results provide evidence that fjords modulate the timing and magnitude of ice sheet  
699 freshwater entering the wider ocean; processes that should be represented in large-scale climate  
700 models if we are to better predict the impact of ice sheet meltwater on the ocean.

701 *Acknowledgments.* We would like to acknowledge Margaret Lindeman for helpful discussion  
702 and suggestions. We acknowledge Clark Richards, Rebecca Jackson, Sarah Das, Jeff Pietro and  
703 others for help in collection of the data. RS and FS acknowledge funding from the NSF. DAS  
704 acknowledges support from NERC Independent Research Fellowship NE/T011920/1. We would  
705 also like to acknowledge the comments of two anonymous reviewers who greatly improved the  
706 manuscript.

707 *Data availability statement.* Data for 2013 is available through the NSF Arctic Data Center at  
708 the following DOIs: 2013 Ship-based ADCP measurements (doi:10.18739/A2P843W9W); 2013  
709 CTD profiles (doi:10.18739/A2B853H78). The 2012 Ship-based ADCP and CTD measurements  
710 are available through the NOAA National Centers for Environmental Information (NCEI) using  
711 NCEI Accession Number 0210572. Additional DOIs for the moored ADCP data and pressure data  
712 are coming soon. The subglacial meltwater discharge data is available from Mankoff et al. (2020).  
713 Python notebooks to run the box model are available upon request.

## 714 **References**

715 Arrigo, K. R., and Coauthors, 2017: Melting glaciers stimulate large summer phytoplankton  
716 blooms in southwest greenland waters. *Geophys. Res. Lett.*, **44**, 6278–6285, <https://doi.org/10.1002/2017GL073583>.

718 Babson, A. L., M. Kawase, and P. MacCready, 2006: Seasonal and Interannual Variability in  
719 the Circulation of Puget Sound, Washington: A Box Model Study. *Atmos.–Ocean*, **44**, 29–45,  
720 <https://doi.org/10.3137/ao.440103>.

721 Bamber, J. L., M. Oppenheimer, R. E. Kopp, W. P. Aspinall, and R. M. Cooke, 2019: Ice Sheet  
722 Contributions to Future Sea-Level Rise from Structured Expert Judgment. *Proc. Natl. Acad.*  
723 *Sci.*, **116**, 11 195–200, <https://doi.org/10.1073/pnas.1817205116>.

724 Bamber, J. L., R. M. Westaway, B. Marzeion, and B. Wouters, 2018: The land ice contribution  
725 to sea level during the satellite era. *Environ. Res. Lett.*, **13**, 063 008, <https://doi.org/10.1088/1748-9326/aac2f0>.

727 Beaird, N., F. Straneo, and W. Jenkins, 2015: Spreading of greenland meltwaters in the  
728 ocean revealed by noble gases. *Geophys. Res. Lett.*, **42**, 7705–7713, <https://doi.org/10.1002/2015GL065003>.

730 Beaird, N., F. Straneo, and W. Jenkins, 2017: Characteristics of meltwater export from jakobshavn  
731 isbræ and ilulissat icefjord. *Ann. of Glaciol.*, **58**, 107–117, <https://doi.org/10.1017/aog.2017.19>.

732 Beaird, N., F. Straneo, and W. Jenkins, 2018: Export of Strongly Diluted Greenland Melt-  
733 water From a Major Glacial Fjord. *Geophys. Res. Lett.*, **45**, 4163–4170, <https://doi.org/10.1029/2018GL077000>.

735 Bendtsen, J., J. Mortensen, K. Lennert, and S. Rysgaard, 2015: Heat sources for glacial ice melt  
736 in a west Greenland tidewater outlet glacier fjord: The role of subglacial freshwater discharge.  
737 *Geophys. Res. Lett.*, **42**, 4089–4095, <https://doi.org/10.1002/2015GL063846>.

738 Bendtsen, J., S. Rysgaard, D. F. Carlson, L. Meire, and M. K. Sejr, 2021: Vertical Mixing in  
739 Stratified Fjords Near Tidewater Outlet Glaciers Along Northwest Greenland. *J. Geophys. Res.*  
740 *Oceans*, **126**, e2020JC016898, <https://doi.org/10.1029/2020JC016898>.

741 Böning, C. W., E. Behrens, A. Biastoch, K. Getzlaff, and J. L. Bamber, 2016: Emerging impact  
742 of greenland meltwater on deepwater formation in the north atlantic ocean. *Nat. Geosci.*, **9**,  
743 523–527, <https://doi.org/10.1038/ngeo2740>.

744 Cape, M. R., F. Straneo, N. Beaird, R. M. Bundy, and M. A. Charette, 2019: Nutrient release  
745 to oceans from buoyancy-driven upwelling at Greenland tidewater glaciers. *Nat. Geosci.*, **12**,  
746 34–39, <https://doi.org/10.1038/s41561-018-0268-4>.

747 Carroll, D., D. A. Sutherland, E. L. Shroyer, J. D. Nash, G. A. Catania, and L. A. Stearns, 2017:  
748 Subglacial discharge-driven renewal of tidewater glacier fjords. *J. Geophys. Res. Oceans*, **122**,  
749 6611–6629, <https://doi.org/10.1002/2017JC012962>.

750 Carroll, D., and Coauthors, 2018: Subannual and Seasonal Variability of Atlantic-Origin Waters in  
751 Two Adjacent West Greenland Fjords. *J. Geophys. Res. Oceans*, **123**, 6670–6687, <https://doi.org/10.1029/2018JC014278>.

753 Cokelet, E. D., and R. J. Stewart, 1985: The exchange of water in fjords: The efflux/reflux theory  
754 of advective reaches separated by mixing zones. *J. Geophys. Res. Oceans*, **90**, 7287–7306,  
755 <https://doi.org/10.1029/JC090iC04p07287>.

756 Davison, B. J., T. R. Cowton, F. R. Cottier, and A. J. Sole, 2020: Iceberg melting substantially  
757 modifies oceanic heat flux towards a major Greenlandic tidewater glacier. *Nat. Commun.*, **11**,  
758 5983, <https://doi.org/10.1038/s41467-020-19805-7>.

759 De Andrés, E., D. A. Slater, F. Straneo, J. Otero, S. Das, and F. Navarro, 2020: Surface emergence  
760 of glacial plumes determined by fjord stratification. *Cryosphere Discuss.*, 1–41, <https://doi.org/10.5194/tc-2019-264>.

761 762 Delhasse, A., C. Kittel, C. Amory, S. Hofer, D. van As, R. S. Fausto, and X. Fettweis, 2020: Brief  
763 communication: Evaluation of the near-surface climate in ERA5 over the Greenland Ice Sheet.  
764 *Cryosphere*, **14**, 957–965, <https://doi.org/10.5194/tc-14-957-2020>.

765 766 Dukhovskoy, D., I. Yashayaev, A. Proshutinsky, J. L. Bamber, I. L. Bashmachnikov, E. P. Chas-  
767 signet, C. M. Lee, and A. J. Tedstone, 2019: Role of greenland freshwater anomaly in the  
768 recent freshening of the subpolar north atlantic. *J. Geophys. Res. Oceans*, **124**, 3333–3360,  
<https://doi.org/10.1029/2018JC014686>.

769 770 Erofeeva, S., and G. Egbert, 2020: Arc5km2018: Arctic ocean inverse tide model on a 5 kilometer  
grid, 2018. *Dataset*, <https://doi.org/10.18739/A21R6N14K>.

771 772 Ezhova, E., C. Cenedese, and L. Brandt, 2016: Interaction between a Vertical Turbulent Jet and a  
Thermocline. *J. Phys. Oceanogr.*, **46**, 3415–3437, <https://doi.org/10.1175/JPO-D-16-0035.1>.

773 774 Ezhova, E., C. Cenedese, and L. Brandt, 2017: Dynamics of a Turbulent Buoyant Plume in a  
Stratified Fluid: An Idealized Model of Subglacial Discharge in Greenland Fjords. *J. Phys.*  
775 *Oceanogr.*, **47**, 2611–2630, <https://doi.org/10.1175/JPO-D-16-0259.1>.

776 777 Fettweis, X., and Coauthors, 2017: Reconstructions of the 1900–2015 Greenland ice sheet  
surface mass balance using the regional climate MAR model. *Cryosphere*, **11**, 1015–1033,  
778 <https://doi.org/10.5194/tc-11-1015-2017>.

779 780 Frajka-Williams, E., J. Bamber, and K. Våge, 2016: Greenland melt and the atlantic meridional  
overturning circulation. *Oceanogr.*, **29**, 22–33, <https://doi.org/10.5670/oceanog.2016.96>.

781 Geyer, W. R., and P. MacCready, 2014: The Estuarine Circulation. *Annu. Rev. Fluid Mech.*, **46**,  
782 175–197, <https://doi.org/10.1146/annurev-fluid-010313-141302>.

783 Giddings, S. N., and P. MacCready, 2017: Reverse Estuarine Circulation Due to Local and Remote  
784 Wind Forcing, Enhanced by the Presence of Along-Coast Estuaries. *J. Geophys. Res. Oceans*,  
785 **122**, 10 184–10 205, <https://doi.org/10.1002/2016JC012479>.

786 Gillibrand, P. A., M. E. Inall, E. Portilla, and P. Tett, 2013: A box model of the seasonal exchange  
787 and mixing in Regions of Restricted Exchange: Application to two contrasting Scottish inlets.  
788 *Environ. Model. Softw.*, **43**, 144–159, <https://doi.org/10.1016/j.envsoft.2013.02.008>.

789 Gladish, C. V., D. M. Holland, A. Rosing-Asvid, J. W. Behrens, and J. Boje, 2014: Oceanic  
790 boundary conditions for Jakobshavn Glacier. Part I: Variability and renewal of Ilulissat Icefjord  
791 Waters, 2001–14. *J. Phys. Oceanogr.*, **45**, 3–32, <https://doi.org/10.1175/JPO-D-14-0044.1>.

792 Goelzer, H., and Coauthors, 2020: The future sea-level contribution of the Greenland ice sheet:  
793 a multi-model ensemble study of ISMIP6. *Cryosphere Discuss.*, 1–43, <https://doi.org/10.5194/tc-2019-319>.

794 Hager, A. O., D. A. Sutherland, J. M. Amundson, R. H. Jackson, C. Kienholz, R. J. Motyka, and J. D.  
795 Nash, 2022: Subglacial discharge reflux and buoyancy forcing drive seasonality in a silled glacial  
796 fjord. *J. Geophys. Res. Oceans*, **127**, e2021JC018355, <https://doi.org/10.1029/2021JC018355>.

797 Hendry, K. R., N. Briggs, S. Henson, J. Opher, J. A. Brearley, M. P. Meredith, M. J.  
798 Leng, and L. Meire, 2021: Tracing Glacial Meltwater From the Greenland Ice Sheet to  
799 the Ocean Using Gliders. *J. Geophys. Res. Oceans*, **126**, e2021JC017274, <https://doi.org/10.1029/2021JC017274>.

800 Hopwood, M. J., D. Carroll, T. J. Browning, L. Meire, J. Mortensen, S. Krisch, and E. P. Achterberg,  
801 2018: Non-linear response of summertime marine productivity to increased meltwater discharge  
802 around Greenland. *Nat. Commun.*, **9**, 1–9, <https://doi.org/10.1038/s41467-018-05488-8>.

803 Hopwood, M. J., and Coauthors, 2020: Review article: How does glacier discharge affect ma-  
804 rine biogeochemistry and primary production in the Arctic? *Cryosphere*, **14**, 1347–1383,  
805 <https://doi.org/10.5194/tc-14-1347-2020>.

808 Inall, M. E., T. Murray, F. R. Cottier, K. Scharrer, T. J. Boyd, K. J. Heywood, and S. L. Be-  
809 van, 2014: Oceanic heat delivery via Kangerdlugssuaq Fjord to the south-east Greenland ice  
810 sheet. *J. Geophys. Res.: Oceans*, **119**, 631–645, <https://doi.org/10.1002/2013JC009295>, eprint:  
811 <https://onlinelibrary.wiley.com/doi/pdf/10.1002/2013JC009295>.

812 Jackson, R. H., S. J. Lentz, and F. Straneo, 2018: The Dynamics of Shelf Forcing in Greenlandic  
813 Fjords. *J. Phys. Oceanogr.*, **48**, 2799–2827, <https://doi.org/10.1175/JPO-D-18-0057.1>.

814 Jackson, R. H., and F. Straneo, 2016: Heat, Salt, and Freshwater Budgets for a Glacial Fjord in  
815 Greenland. *J. Phys. Oceanogr.*, **46**, 2735–2768, <https://doi.org/10.1175/JPO-D-15-0134.1>.

816 Jackson, R. H., F. Straneo, and D. A. Sutherland, 2014: Externally forced fluctuations in ocean tem-  
817 perature at Greenland glaciers in non-summer months. *Nat. Geosci.*, **7**, 503–508, <https://doi.org/10.1038/ngeo2186>.

819 Jackson, R. H., and Coauthors, 2017: Near-glacier surveying of a subglacial discharge plume:  
820 Implications for plume parameterizations. *Geophys. Res. Lett.*, **44**, 6886–6894, <https://doi.org/10.1002/2017GL073602>.

822 Jenkins, A., 2011: Convection-Driven Melting near the Grounding Lines of Ice Shelves and  
823 Tidewater Glaciers. *J. Phys. Oceanogr.*, **41**, 2279–2294, <https://doi.org/10.1175/JPO-D-11-03.1>.

824 Klymak, J. M., and M. C. Gregg, 2004: Tidally Generated Turbulence over the Knight In-  
825 let Sill. *J. Phys. Oceanogr.*, **34**, 1135–1151, [https://doi.org/10.1175/1520-0485\(2004\)034<1135:TGTOTK>2.0.CO;2](https://doi.org/10.1175/1520-0485(2004)034<1135:TGTOTK>2.0.CO;2).

827 Le Bras, I., F. Straneo, M. Muilwijk, L. H. Smedsrød, F. Li, M. S. Lozier, and N. P. Holliday,  
828 2021: How much arctic fresh water participates in the subpolar overturning circulation? *J. Phys.*  
829 *Oceanogr.*, **51**, 955–973, <https://doi.org/10.1175/jpo-d-20-0240.1>.

830 MacCready, P., and Coauthors, 2021: Estuarine Circulation, Mixing, and Residence Times  
831 in the Salish Sea. *J. Geophys. Res. Oceans*, **126**, e2020JC016738, <https://doi.org/10.1029/2020JC016738>.

833 Mankoff, K. D., F. Straneo, C. Cenedese, S. B. Das, C. G. Richards, and H. Singh, 2016: Structure  
834 and dynamics of a subglacial discharge plume in a greenlandic fjord. *J. Geophys. Res.: Oceans*,  
835 **121**, 8670–8688, <https://doi.org/10.1002/2016JC011764>.

836 Mankoff, K. D., and Coauthors, 2020: Greenland liquid water discharge from 1958 through 2019.  
837 *Earth Syst. Sci. Data*, **12**, 2811–2841, <https://doi.org/10.5194/essd-12-2811-2020>, publisher:  
838 Copernicus GmbH.

839 McDougall, T. J., and P. M. Barker, 2011: *Getting started with TEOS-10 and the Gibbs Seawater*  
840 (*GSW*) *Oceanographic Toolbox*. SCOR/IAPSO WG127, 28 pp.

841 Meire, L., J. Mortensen, S. Rysgaard, J. Bendtsen, W. Boone, P. Meire, and F. J. R. Meysman,  
842 2016a: Spring bloom dynamics in a subarctic fjord influenced by tidewater outlet glaciers  
843 (Godthåbsfjord, SW Greenland). *J. Geophys. Res. Biogeosci.*, **121**, 1581–1592, <https://doi.org/10.1002/2015JG003240>.

845 Meire, L., and Coauthors, 2016b: High export of dissolved silica from the Greenland Ice Sheet.  
846 *Geophys. Res. Lett.*, **43**, 9173–9182, <https://doi.org/10.1002/2016GL070191>.

847 Meire, L., and Coauthors, 2017: Marine-terminating glaciers sustain high productivity in greenland  
848 fjords. *Glob. Change Biol.*, **23**, 5344–5357, <https://doi.org/10.1111/gcb.13801>.

849 Mernild, S. H., D. M. Holland, D. Holland, A. Rosing-Asvid, J. C. Yde, G. E. Liston, and  
850 K. Steffen, 2015: Freshwater Flux and Spatiotemporal Simulated Runoff Variability into Ilulissat  
851 Icefjord, West Greenland, Linked to Salinity and Temperature Observations near Tidewater  
852 Glacier Margins Obtained Using Instrumented Ringed Seals. *J. Phys. Oceanogr.*, **45**, 1426–  
853 1445, <https://doi.org/10.1175/JPO-D-14-0217.1>.

854 Moon, T., D. A. Sutherland, D. Carroll, D. Felikson, L. Kehrl, and F. Straneo, 2018: Subsurface  
855 iceberg melt key to Greenland fjord freshwater budget. *Nat. Geosci.*, **11**, 49–54, <https://doi.org/10.1038/s41561-017-0018-z>.

857 Morlighem, M., and Coauthors, 2017: BedMachine v3: Complete Bed Topography and Ocean  
858 Bathymetry Mapping of Greenland From Multibeam Echo Sounding Combined With Mass  
859 Conservation. *Geophys. Res. Lett.*, **44**, 11,051–11,061, <https://doi.org/10.1002/2017GL074954>.

860 Mortensen, J., J. Bendtsen, K. Lennert, and S. Rysgaard, 2014: Seasonal variability of the  
861 circulation system in a west Greenland tidewater outlet glacier fjord, Godthåbsfjord (64°N). *J.*  
862 *Geophys. Res. Earth Surf.*, **119**, 2591–2603, <https://doi.org/10.1002/2014JF003267>.

863 Mortensen, J., J. Bendtsen, R. J. Motyka, K. Lennert, M. Truffer, M. Fahnestock, and S. Rysgaard,  
864 2013: On the seasonal freshwater stratification in the proximity of fast-flowing tidewater outlet  
865 glaciers in a sub-Arctic sill fjord. *J. Geophys. Res. Oceans*, **118**, <https://doi.org/10.1002/jgrc.2134>.

867 Mortensen, J., K. Lennert, J. Bendtsen, and S. Rysgaard, 2011: Heat sources for glacial melt in  
868 a sub-arctic fjord (godthåbsfjord) in contact with the greenland ice sheet. **116**, <https://doi.org/10.1029/2010JC006528>.

870 Mortensen, J., S. Rysgaard, K. E. Arendt, T. Juul-Pedersen, D. H. Søgaard, J. Bendtsen, and  
871 L. Meire, 2018: Local Coastal Water Masses Control Heat Levels in a West Greenland Tidewater  
872 Outlet Glacier Fjord. *J. Geophys. Res. Oceans*, **123**, <https://doi.org/10.1029/2018JC014549>.

873 Mortensen, J., S. Rysgaard, J. Bendtsen, K. Lennert, T. Kanzow, H. Lund, and L. Meire,  
874 2020: Subglacial Discharge and Its Down-Fjord Transformation in West Greenland Fjords  
875 With an Ice Mélange. *J. Geophys. Res. Oceans*, **125**, e2020JC016301, <https://doi.org/10.1029/2020JC016301>.

877 Mortensen, J., S. Rysgaard, M. H. S. Winding, T. Juul-Pedersen, K. E. Arendt, H. Lund, A. E.  
878 Stuart-Lee, and L. Meire, 2022: Multidecadal Water Mass Dynamics on the West Greenland  
879 Shelf. *J. Geophys. Res. Oceans*, **127**, e2022JC018724, <https://doi.org/10.1029/2022JC018724>.

880 Motyka, R. J., M. Truffer, M. Fahnestock, J. Mortensen, S. Rysgaard, and I. Howat, 2011: Sub-  
881 marine melting of the 1985 Jakobshavn Isbræ floating tongue and the triggering of the current  
882 retreat. *J. Geophys. Res. Earth Surf.*, **116**, <https://doi.org/10.1029/2009JF001632>.

883 Muilwijk, M., F. Straneo, D. A. Slater, L. H. Smedsrød, J. Holte, M. Wood, C. S. Andresen, and  
884 B. Harden, 2022: Export of Ice Sheet Meltwater from Upernivik Fjord, West Greenland. *J.  
885 Phys. Oceanogr.*, **52**, 363–382, <https://doi.org/10.1175/JPO-D-21-0084.1>.

886 Nghiem, S. V., and Coauthors, 2012: The extreme melt across the Greenland ice sheet in 2012.  
887 *Geophys. Res. Lett.*, **39**, <https://doi.org/10.1029/2012GL053611>.

888 Oksman, M., and Coauthors, 2022: Impact of freshwater runoff from the southwest Greenland Ice  
889 Sheet on fjord productivity since the late 19th century. *Cryosphere Discuss.*, 1–28, <https://doi.org/10.5194/tc-2021-373>.

891 Oliver, H., R. M. Castelao, C. Wang, and P. L. Yager, 2020: Meltwater-Enhanced Nutrient  
892 Export From Greenland's Glacial Fjords: A Sensitivity Analysis. *J. Geophys. Res. Oceans*, **125**,  
893 e2020JC016185, <https://doi.org/10.1029/2020JC016185>.

894 Padman, L., and S. Erofeeva, 2004: A barotropic inverse tidal model for the Arctic Ocean. *Geophys.*  
895 *Res. Lett.*, **31**, <https://doi.org/10.1029/2003GL019003>.

896 Podolskiy, E. A., N. Kanna, and S. Sugiyama, 2021: Co-seismic eruption and intermittent tur-  
897 bulence of a subglacial discharge plume revealed by continuous subsurface observations in  
898 Greenland. *Commun. Earth Environ.*, **2**, 1–16, <https://doi.org/10.1038/s43247-021-00132-8>.

899 Rysgaard, S., and Coauthors, 2020: An Updated View on Water Masses on the  
900 pan-West Greenland Continental Shelf and Their Link to Proglacial Fjords. *Journal*  
901 *of Geophysical Research: Oceans*, **125** (2), e2019JC015564, <https://doi.org/10.1029/2019JC015564>, URL <https://onlinelibrary.wiley.com/doi/abs/10.1029/2019JC015564>, eprint:  
902 <https://onlinelibrary.wiley.com/doi/pdf/10.1029/2019JC015564>.

903 Schaffer, J., T. Kanzow, W.-J. von Appen, L. von Albedyll, J. E. Arndt, and D. H. Roberts, 2020:  
904 Bathymetry constrains ocean heat supply to greenland's largest glacier tongue. **13** (3), 227–231,  
905 <https://doi.org/10.1038/s41561-019-0529-x>.

906 Slater, D. A., F. Straneo, S. B. Das, C. G. Richards, T. J. W. Wagner, and P. W. Nienow, 2018:  
907 Localized plumes drive front-wide ocean melting of a greenlandic tidewater glacier. *Geophys.*  
908 *Res. Lett.*, **45**, 12,350–12,358, <https://doi.org/10.1029/2018GL080763>.

909 Staalstrøm, A., L. Arneborg, B. Liljebladh, and G. Broström, 2015: Observations of Turbulence  
910 Caused by a Combination of Tides and Mean Baroclinic Flow over a Fjord Sill. *J. Phys.*  
911 *Oceanogr.*, **45**, 355–368, <https://doi.org/10.1175/JPO-D-13-0200.1>.

912 Stevens, L. A., F. Straneo, S. B. Das, A. J. Plueddemann, A. L. Kukulya, and M. Morlighem, 2016:  
913 Linking glacially modified waters to catchment-scale subglacial discharge using autonomous  
914 underwater vehicle observations. *Cryosphere*, **10**, 417–432, <https://doi.org/https://doi.org/10.5194/tc-10-417-2016>.

915 Straneo, F., and C. Cenedese, 2015: The dynamics of greenland's glacial fjords and their role in cli-  
916 mate. *Annu. Rev. Mar. Sci.*, **7**, 89–112, <https://doi.org/10.1146/annurev-marine-010213-135133>.

919 Straneo, F., and Coauthors, 2019: The case for a sustained Greenland Ice Sheet-Ocean observing  
920 system (GrIOOS). *Front. Mar. Sci.*, **6**, <https://doi.org/10.3389/fmars.2019.00138>.

921 Stuart-Lee, A. E., J. Mortensen, A.-S. v. d. Kaaden, and L. Meire, 2021: Seasonal Hydrography of  
922 Ameralik: A Southwest Greenland Fjord Impacted by a Land-Terminating Glacier. *J. Geophys.*  
923 *Res. Oceans*, **126**, e2021JC017552, <https://doi.org/10.1029/2021JC017552>.

924 Sutherland, D. A., F. Straneo, and R. S. Pickart, 2014: Characteristics and dynamics of two  
925 major Greenland glacial fjords. *J. Geophys. Res. Oceans*, **119**, 3767–3791, <https://doi.org/10.1002/2013JC009786>.

926 Tedesco, M., X. Fettweis, T. Mote, J. Wahr, P. Alexander, J. E. Box, and B. Wouters, 2013: Evidence  
927 and analysis of 2012 greenland records from spaceborne observations, a regional climate model  
928 and reanalysis data. **7**, 615–630, <https://doi.org/https://doi.org/10.5194/tc-7-615-2013>.

929 Thornalley, D. J., and Coauthors, 2018: Anomalously weak Labrador Sea convection and At-  
930 lantic overturning during the past 150 years. *Nature*, **556**, 227–230, <https://doi.org/10.1038/s41586-018-0007-4>.

931 Valle-Levinson, A., 2008: Density-driven exchange flow in terms of the kelvin and ekman numbers.  
932 *J. Geophys. Res. Oceans*, **113**, <https://doi.org/10.1029/2007JC004144>.

933 Wagner, T. J. W., F. Straneo, C. G. Richards, D. A. Slater, L. A. Stevens, S. B. Das, and H. Singh,  
934 2019: Large spatial variations in the flux balance along the front of a Greenland tidewater glacier.  
935 *Cryosphere*, **13**, 911–925, <https://doi.org/https://doi.org/10.5194/tc-13-911-2019>.

936 Wain, D. J., M. C. Gregg, M. H. Alford, R.-C. Lien, R. A. Hall, and G. S. Carter, 2013: Propagation  
937 and dissipation of the internal tide in upper Monterey Canyon. *J. Geophys. Res. Oceans*, **118**,  
938 <https://doi.org/10.1002/jgrc.20368>.

939 Wood, M., E. Rignot, I. Fenty, D. Menemenlis, R. Millan, M. Morlighem, J. Mouginot, and  
940 H. Seroussi, 2018: Ocean-Induced Melt Triggers Glacier Retreat in Northwest Greenland.  
941 *Geophys. Res. Lett.*, **45**, 8334–8342, <https://doi.org/10.1029/2018GL078024>.

942 Zhao, K. X., A. L. Stewart, and J. C. McWilliams, 2018: Sill-influenced exchange flows in ice  
943 shelf cavities. *J. Phys. Oceanogr.*, **49**, 163–191, <https://doi.org/10.1175/JPO-D-18-0076.1>.

946 Zhao, K. X., A. L. Stewart, and J. C. McWilliams, 2021: Geometric Constraints on  
947 Glacial Fjord–Shelf Exchange. *J. Phys. Oceanogr.*, **51**, 1223–1246, <https://doi.org/10.1175/JPO-D-20-0091.1>.

948

949 Zhao, K. X., A. L. Stewart, and J. C. McWilliams, 2022: Linking Overturning, Recirculation, and  
950 Melt in Glacial Fjords. *Geophys. Res. Lett.*, **49**, <https://doi.org/10.1029/2021GL095706>.